THE KINETICS OF γ COMPLEX, THE *ESCHERICHIA COLI* CLAMP LOADER, BINDING THE β-CLAMP BEFORE DNA DURING THE CLAMP LOADING REACTION

By

JENNIFER A. THOMPSON

A THESIS PRESENTED TO THE GRADUATE SCHOOL
OF THE UNIVERSITY OF FLORIDA IN PARTIAL FULFILLMENT
OF THE REQUIREMENTS FOR THE DEGREE OF
MASTER OF SCIENCE

UNIVERSITY OF FLORIDA

2010

To my family and friends

ACKNOWLEDGMENTS

I thank Dr. Linda Bloom, my mentor, for her helpful guidance, advice, and support as well as Dr. Laipis and Dr. Cain of my supervisory committee for their mentoring. I thank Chris Paschall, Ankita Chiraniya, Jaclyn Hayner, Dr. Melissa Marzahn, and the other members of the Bloom lab over the past three years for their research assistance, thoughtful discussions, and friendship. I also thank the National Institutes of Health for its generous support. I thank my parents and my family for their loving support through all the years and to Chris Meyer for being a constant source of encouragement, motivation, and love.

TABLE OF CONTENTS

page

ACKNOWLEDGMENTS 4

LIST OF FIGURES 7

LIST OF ABBREVIATIONS 9

ABSTRACT 11

CHAPTER

1 INTRODUCTION 13

Escherichia coli DNA Replication 13
Eukaryotic DNA Replication 14
Processivity Factors 16
Structure of Sliding Clamps 16
Structure of Clamp Loaders 17
Clamp Loading Mechanism 20

2 MATERIALS AND METHODS 27

Materials 27
Nucleotides and Oligonucleotides 27
RFC and Rad24-RFC Purification 27
Buffers 27
Methods 28
Purification of DNA Polymerase III Proteins 28
β-Sliding Clamp Mutagenesis 28
β-Sliding Clamp Transformation 28
β-Sliding Clamp Purification 29
Covalent Labeling of the β-clamp with Pyrene 31
PCNA Sliding Clamp Mutagenesis 31
PCNA Sliding Clamp Transformation 32
PCNA Sliding Clamp Purification 33
Covalent Labeling of the PCNA-clamp with AlexaFluor 488 35
Protein Concentrations 36
Labeling Primer DNA with DCC 37
Experimental Procedures 37
Steady State Fluorescence Assays 37
Pre-Steady State Fluorescence Assays 38
Data Analysis 38
Steady State Fluorescence Assays 38
Pre-Steady State Fluorescence Assays 39
Kinetic Modeling 39

3 RESULTS 41

Introduction 41
Equilibrium Binding of γ complex to β 42
Kinetics of γ complex binding β 43
Binding of γ complex to DNA 44
Rates of γ Complex Binding β with and without Preincubation of γ Complex with ATP 45
DNA Binding with and without ATP Preincubation 46
Effect of ATP Concentration on γ Complex•DNA Binding Kinetics 47
Kinetic Modeling of DNA Binding Reactions 48
Discussion 50
Two Sets of ATP-induced Conformational Changes 51
A Kinetic Preference for the Clamp Loader to Bind β before DNA 52

4 DISCUSSION AND FUTURE STUDIES 67

APPENDIX: DEVELOPMENT OF A NEW FLUORESCENCE-BASED ASSAY: MEASURING PCNA OPENING IN THE *SACCHAROMYCES CEREVISIAE* DNA REPLICATION SYSTEM 70

Introduction 70
A fluorescence-intensity based assay to measure opening and closing of an RFC•PCNA complex 71
Measuring Rad24-RFC•PCNA Interactions using the PCNA-AF488 Opening Assay 73
Discussion and Future Studies 74

REFERENCE LIST 81

BIOGRAPHICAL SKETCH 88

LIST OF FIGURES

Figure		page
1-1	A Model of the *Escherichia coli* Replisome.	22
1-2	Structure of sliding clamps.	23
1-3	Structure of the *E. coli* clamp loader, γ complex.	24
1-4	Structure of the *S. cerevisiae* clamp loader, RFC.	25
1-6	The ATP-dependent steps of the clamp loading reaction.	26
3-1	Fluorescence intensity-based β-clamp binding assay.	55
3-2	Emission Spectra of pyrene fluorescence.	56
3-3	Equilibrium binding of γ complex to β.	57
3-4	Kinetics of γ complex binding to β-PY.	58
3-5	Binding of γ complex to DNA.	59
3-6	The rate of γ complex binding to DNA.	60
3-7	Rates of γ complex binding β with and without pre-incubation of γ complex with ATP.	61
3-8	γ complex binding DNA with and without pre-incubation of γ complex with ATP.	62
3-9	Effect of ATPγS preincubation on the rate of γ complex binding p/t-DNA-DCC.	63
3-10	Effect of ATP concentration on γ complex•DNA binding kinetics.	64
3-11	Kinetic model fit to p/t-DNA binding data.	65
3-12	Model for formation of a ternary clamp loader•clamp•DNAcomplex.	66
A-1	Crystal Structural Model of PCNA highlighting the residues mutated for the PCNA opening assay.	76
A-2	Relief of the AF488 Fluorescence quench in the presence of SDS.	77
A-3	Emission spectra of PCNA-AF488 were taken at excitation wavelength of 495 nm.	78

A-4 Equilibrium binding and opening of RFC•PCNA. 79

A-5 Equilibrium binding and opening of Rad24-RFC•PCNA. 80

LIST OF ABBREVIATIONS

AAA+	ATPases associated with cellular activities
AF488	AlexaFluor 488, C_5 maleimide
ATP	adenosine triphosphate
ATPγS	adenosine 5’-O-(thiotriphosphate)
β-PY	β covalently labeled on residue Q299C with pyrene
BSA	bovine serum albumin
DCC	7-diethylaminocoumarin-3-carboxylic acid, succinimidyl ester
DMSO	dimethyl sulfoxide
DNA	deoxyribonucleic acid
E. coli	*Escherichia coli*
GINS	complex of Sld5-Psf1-Psf2-Psf3 (Go-Ichi-Ni-San or 5-1-2-3))
IDCL	interdomain connecting loop
LB	Luria Broth
MCM	mini chromosome maintenance
PAGE	polyacrylamide gel electrophoresis
PCNA	proliferating cell nuclear antigen
PCNA-AF488	PCNA covalently labeled on residues I111C and I181C with AlexaFluor 488
PIP box	PCNA interacting peptide
Pol III	DNA polymerase III
p/t-DNA	primer/template DNA
p/t-DNA-DCC	primed template DNA with an amino linker covalently labeled with DCC
PY	N- (1-pyrene) maleimide

RFC	replication factor C
RNA	ribonucleic acid
SRC	serine arginine cysteine
SSB	single stranded DNA binding protein
TCEP	tris (2-carboxyethyl) phosphine

Abstract of Thesis Presented to the Graduate School
of the University of Florida in Partial Fulfillment of the
Requirements for the Degree of Master of Science

THE KINETICS OF γ COMPLEX, THE *ESCHERICHIA COLI* CLAMP LOADER, BINDING THE β-CLAMP BEFORE DNA DURING THE CLAMP LOADING REACTION

By

Jennifer A. Thompson

May 2010

Chair: Linda Bloom
Major: Biochemistry and Molecular Biology

In *Escherichia coli,* the γ complex clamp loader loads the β-sliding clamp onto DNA. The β clamp tethers DNA polymerase III to DNA and enhances the efficiency of replication by increasing the processivity of DNA synthesis. In the presence of ATP, γ complex binds β and DNA to form a ternary complex. Binding to primed template DNA triggers γ complex to hydrolyze ATP and release the clamp onto DNA. Here, we investigated the kinetics of forming a ternary complex by measuring rates of γ complex binding β and DNA. A fluorescence intensity-based β binding assay was developed in which the fluorescence of pyrene covalently attached to β increases when bound by γ complex. Using this assay, an association rate constant of 2.3×10^7 $M^{-1}s^{-1}$ for γ complex binding β was determined. The rate of β binding was the same in experiments in which γ complex was pre-incubated with ATP before adding β or added directly to β and ATP. In contrast when γ complex is pre-incubated with ATP, DNA binding is faster than when γ complex is added to DNA and ATP at the same time. Slow DNA binding in the absence of ATP pre-incubation is the result of a rate-limiting ATP-induced conformational change. Our results strongly suggest that the ATP-induced conformational changes that promote β binding and DNA binding differ. The slow ATP-

induced conformational change that precedes DNA binding may provide a kinetic preference for γ complex to bind β before DNA during the clamp loading reaction cycle.

CHAPTER 1
INTRODUCTION

Escherichia coli DNA Replication

DNA replication occurs semiconservatively such that each parental DNA strand is replicated in a 5’ to 3’ direction to create two new daughter strands (reviewed in (1)). At the replication fork, a large multicomponent holoenzyme complex simultaneously organizes and coordinates the continuous and discontinuous synthesis of the leading and lagging strands, respectively, of the double helix (reviewed in (2)) (Fig. 1-1). DNA synthesis is initiated when the replicative DNA polymerase extends the 3’ end of an RNA primer. Primase (DnaG), an RNA polymerase, synthesizes these short (10-12 nt) RNA primers (3,4). DnaB, the ring-shaped replicative helicase, unwinds the duplex DNA with 5’-3’ polarity ahead of the replication fork (reviewed in (5,6)). The helicase is bound to both the clamp loader and to primase to stimulate helicase activity at the fork (7,8). On the leading strand, only one RNA primer is required because synthesis is continuous but on the lagging strand multiple primed sites are required for each 1-2 kb DNA segment created called Okazaki fragments. During Okazaki fragment maturation, the 5’ RNA ends are replaced with DNA and the DNA fragments are joined by ligase.

The DNA polymerase III (Pol III) holoenzyme consists of ten subunits that are divided into three separate subassemblies: 1) Pol III core; 2) β-clamp; and 3) DnaX complex clamp loader. Two Pol III cores, one for each DNA strand, are required at the replication fork (9-11). The core is a heterotrimer consisting of the α subunit which has DNA polymerase activity, the ε subunit which functions in proofreading and has 3’-5’ exonuclease activity, and the θ subunit which has an unknown function. The two Pol III

cores on the leading and lagging strands are linked together by the τ subunits of the clamp loader.

Without the help of accessory proteins, the Pol III core incorporates only approximately 20 nucleotides in a single DNA binding event and can easily dissociate from the template. Sliding clamps and clamp loaders enhance the processivity of DNA synthesis (12). Clamps encircle DNA while tethering DNA polymerases to the DNA template and freely slide along with the polymerase in either direction (13). The addition of clamps increases the processivity of replicative DNA polymerases from tens to thousands of nucleotides per DNA binding event (14). ATP-dependent clamp loaders are required to actively open and close the sliding clamps onto DNA. Only one clamp is required on the leading strand where DNA replication is continuous but the lagging strand synthesizes DNA discontinuously and requires a new clamp to be loaded per Okazaki fragment made. Clamp loading on the lagging strand must be fast since typically 1 kb of DNA is synthesized per second and must be coordinated with the leading strand synthesis.

Eukaryotic DNA Replication

In eukaryotes, the process of DNA replication is much more complex and many of the mechanisms are not well known. There are many more components, including over 15 DNA polymerases, involved in the replication and repair pathways (10). Although eukaryotic replication may be more complex than bacterial replication, the core proteins in the replisome are more analogous than different in both structure and function. Leading strand synthesis begins with the primase activity of DNA polymerase α/primase laying down an 8-10 nt RNA primer. The DNA polymerase subunit of DNA pol

α/primase extends the RNA primer with DNA creating an RNA-DNA hybrid. The eukaryotic helicase is thought to be a hetero-oligomeric complex consisting of a Cdc45/MCM/GINS (CMG) complex, although the exact composition of the active helicase is still unclear (15-18). The CMG complex unwinds with 3’ to 5’ polarity, which is the opposite of the bacterial DnaB helicase. Replication factor C (RFC), the eukaryotic clamp loader, loads the sliding clamp, proliferating cell nuclear antigen (PCNA), onto the 3’ end of the RNA-DNA primer, which displaces DNA pol α/primase. The leading strand polymerase, which is thought to be DNA pol ε, then binds to PCNA once RFC dissociates and processive synthesis can continue (19).

Eukaryotic Okazaki fragments are about 10-fold smaller than the bacterial counterparts and are made at a rate 10-fold slower at the replication fork. Synthesis of the lagging strand starts in a similar way with DNA pol α/primase creating RNA-DNA hybrid primers but a new primer is needed every 100-200 nt for each new Okazaki fragment. RFC loads a new PCNA sliding clamp per DNA fragment being created. In comparison with the leading strand, DNA pol δ is the polymerase thought to be on the lagging strand that associates with the clamp and allows for processive synthesis (20,21). Okazaki fragment maturation occurs when a ribonuclease, typically RNaseHI, removes all of the RNA in the primer except for the last RNA nucleotide, which is removed by flap endonuclease-1 (FEN-1) (22). Other pathways to degrade the primer, depending on the structure of the 5’ end of the Okazaki fragment, can occur including those that involve Dna2 (23). DNA pol δ fills in the gap and DNA ligase joins the Okazaki fragments together.

Processivity Factors

Structure of Sliding Clamps

The overall structure and function of sliding clamps are conserved from bacteria to humans (reviewed in (10,24)). Most clamps are ring-shaped complexes composed of identical protein subunits (13,25,26). The *E. coli* β-sliding clamp is a dimer composed of two identical protein monomers while both the *Saccharomyces cerevisiae* and human PCNA sliding clamps are trimers (Fig. 1-2A-C). Although there is little sequence homology between the bacterial and eukaryotic clamps, both β and PCNA contain six globular domains with a comparable fold that are linked by interdomain connecting loops (IDCL). The β-clamp has three domains per subunit creating two interfaces while PCNA has two domains per subunit creating three interfaces. Due to the uniform clamp structure, the clamp loader can in principle open any interface pair on the clamp to allow DNA to pass through the center of the ring.

The subunits of sliding clamps are arranged in a head-to-tail fashion giving clamps a rotational axis of symmetry through the center of the ring, and two distinct faces. Theoretically, proteins can bind either face of the clamp but it has been found that most proteins bind the same face, the face in which the C-termini protrude (27,28). The inner part of the ring is a surface of 12 positively charged α-helices, which encircles the DNA and the outer portion of the clamp is mostly composed of β sheets. The β-clamp has a central opening of 35 Å in diameter and is approximately 34 Å thick allowing the ring to cover one helical turn of DNA when bound. PCNA has a similar diameter of about 34 Å for the central opening and a thickness of about 30Å.

DNA sliding clamps have been found to be involved in almost all processes related with DNA metabolism including replication, repair, and modification. Clamps

have been found to interact with a variety of proteins and protein complexes during these processes. Many proteins that bind clamps interact through a conserved peptide sequence motif. Based on sequence alignments and binding studies, this motif is proposed to be QxxL (x) F for the β-clamp and Qxx (I/L/M) xxF (F/Y) for PCNA, termed the PCNA Interacting Peptide box (PIP box) (29-31). PCNA has been found to bind cell cycle regulators, repair enzymes, and protein kinases among others. The PIP-box folds into a 3_{10} helix and has 3 residues per turn, which differs slightly from an α helix, which has 3.6 residues per turn. An important feature of this binding motif is the presence of hydrophobic amino acid residues including phenylalanine and tyrosine, which come in contact with the hydrophobic pocket on the clamp under an IDCL (32-34). Sliding clamps have one hydrophobic binding pocket per monomer therefore PCNA has three while there are two binding pockets on the β-clamp. Recent work has shown that more than one protein can be bound to β or PCNA at a time (reviewed in (35)). The sliding clamp tool belt model suggests that more than one DNA polymerase binds to the β-clamp at once to facilitate polymerase switching (36). The clamp loader and the replicative DNA polymerase are not able to bind the clamp at the same time even though other proteins may be able to bind a different pocket. Steric effects require the clamp loader to dissociate from the clamp before the polymerase can bind and proceed with replication (27,28,34,37).

Structure of Clamp Loaders

Clamp loaders are multi-subunit, spiral-shaped complexes of similarly structured proteins that are part of the AAA+ family of ATPases (38-42). The ATPase regions of the clamp loader use ATP binding and hydrolysis to promote molecular interactions that catalyze the different steps of the clamp loading mechanism. Each subunit of the clamp

loader contains three domains joined by flexible linkers. Domains I and II located at the N-terminal region are structurally conserved and form the AAA+ family of ATPase region while domain III at the C-terminal end is unique to clamp loaders (43) (Figure 1-3A). An active clamp loader consists of five subunits and is held tightly together at the C-terminal domains to form a collar while the N-terminal domains are more loosely suspended with the A and E subunits not touching at all creating an open area (33,44,45) (Figure 1-3B). This gap could potentially allow DNA to enter the central chamber in the clamp loader, which positions DNA into the open clamp. The clamp is opened into a right-handed helix and fits the spiral of the clamp loader (33,46). Electron microscopy studies of archaeal RFC•PCNA•DNA•ATPγS complex reveal PCNA in an open lock-washer appearance that allows the clamp to dock on the surface of the helical RFC (47).

At the replication fork, the *E. coli* clamp loader is comprised of seven subunits, including three copies of the *dnaX* gene, δ, δ', χ, and ψ (45,48,49). The *dnaX* gene produces τ, the full-length product, and a truncated form, γ, which results from a translational frameshift. The γ subunit is approximately ⅔ the length of τ and has identical sequence except for the last amino acid (50-52). The C-terminal extension on τ coordinates the activity of the DNA polymerase at the replication fork by binding to the α subunit of the core polymerase as well as to the DnaB helicase (11,53). In cells, the clamp loader with the composition, $\tau_2\gamma\delta\delta'\chi\psi$, has been isolated and was found tethered to two copies of the core polymerase. The clamp loader with this specific composition is thought to be the main clamp loader in the holoenzyme complex. Clamp loaders with various combinations of τ and γ subunits are shown to be fully active in clamp loading

but not in processive replication *in vitro* (48). The five subunit core, $DnaX_3\delta\delta'$ termed the minimal complex, is an active clamp loader but less efficient than the seven subunit complex (54-56).

In the clamp loader, the three DnaX subunits bind and hydrolyze ATP and are often thought of as the “motor” due to the ATPase activity (56-58). The δ subunit interacts with the β-clamp and is called the “wrench” because this subunit alone can open the clamp to unload from DNA (59,60). Unlike the rest of the subunits, the δ’ subunit is thought to be stationary and helps control the δ-β interaction. The ψ subunit stabilizes the clamp loader-clamp complex while the χ subunit interacts with single stranded DNA binding protein (SSB) and increases the efficiency of clamp loading (55,61,62).

RFC, the eukaryotic clamp loader, consists of five subunits that are found in a similar arrangement to that of the bacterial clamp loader. The yeast and human clamp loaders are composed of four small subunits and one large subunit, which has additional N-terminal and C-terminal extensions that are not present in the small subunits (63-65) (Figure 1-4A-B). The exact function of these two additional regions is not yet known. The N-terminal region (removed from structure in Fig. 1-4) binds to DNA but is not directly required for clamp loading and deletion of this region increases clamp loading activity *in vitro* and cells are still viable *in vivo* (66-68). All five subunits are part of the AAA+ family of ATPases but only subunits 1-4 (A-D) are functional. RFC1 (A) is analogous to the δ subunit in the *E. coli* clamp loader but is a functional ATPase unlike its bacterial counterpart (69,70). RFC5 (E) is analogous to the δ’ subunit in that it cannot hydrolyze ATP but the subunit does have an arginine finger that can interact with the

ATP site of the adjacent subunit, RFC2. The remaining subunits, RFC2-4 (B-D), are similar to the three γ subunits of γ complex and are functional ATPases.

In all species of clamp loaders, the ATP sites are located at the interfaces of the clamp loader subunits and contain conserved Walker A and Walker B sequence motifs. An arginine finger residue located in a conserved Ser-Arg-Cys (SRC) motif reaches into the interface of the ATP site of the adjacent subunit and senses when ATP is bound (71,72). This location may enable the subunits to undergo conformational changes in response to ATP binding and hydrolysis, which would allow the clamp loader into interact with the other molecules. Different conformational states formed by the clamp loader may drive different steps in the clamp loading mechanism. There are slight differences between these systems in how the ATP sites fill and when hydrolysis occurs. Binding studies with yeast RFC show that the ATP sites fill sequentially. Using ATPγS to characterize the ATP binding steps, it was shown that two molecules of ATPγS promotes binding of either PCNA or DNA, and binding of PCNA or DNA promotes binding of a third molecule of ATPγS. The formation of a ternary RFC–PCNA–DNA complex promotes binding a fourth ATPγS molecule. In contrast to yeast, all three sites in the *E. coli* γ complex bind ATP in the absence of the clamp or DNA.

Clamp Loading Mechanism

Clamp loading is a dynamic process, which includes many different steps that lead to the formation of a ternary complex and ultimately the assembly of the clamp onto DNA (Figure 1-5). The clamp loader must first be primed with ATP and undergo a conformational change that increases its affinity for binding the clamp (27,73,74). The ATP-primed clamp loader can bind to either the clamp or to DNA first and ultimately form a ternary clamp loader-clamp-DNA complex. The binding of the clamp loader to

DNA triggers hydrolysis of ATP in one or more of the ATP sites (75,76). Hydrolysis of ATP most likely causes another conformational change in the clamp loader prompting it to lose affinity for the clamp and DNA. The sliding clamp is closed around DNA and the clamp loader dissociates from the complex. All these steps must occur rapidly and in a defined order to allow the processive DNA polymerase to then bind and proceed with elongation. Although there have been many recent developments in this complex mechanism, there are still many questions left to be answered.

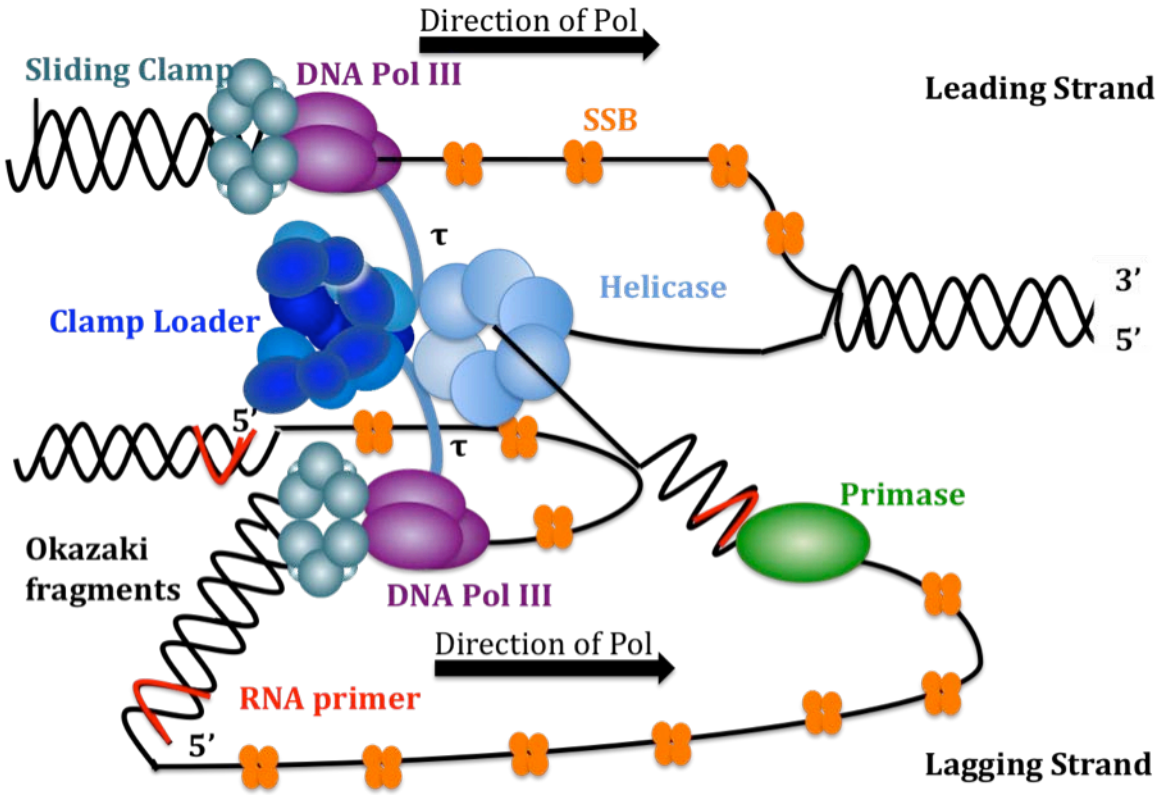

Figure 1-1. A Model of the *Escherichia coli* Replisome. The *E. coli* replisome uses two Pol III core enzymes (purple) to copy leading and lagging strands. The replicative helicase (light blue) unwinds duplex DNA ahead of the replication fork and stimulates primase activity. Primase (green) synthesizes short RNA primers for each Okazaki fragment. The β sliding clamps (gray) give processivity to the Pol III core by tethering the polymerase to the DNA template. The clamp loader, (blue) uses the energy of ATP hydrolysis to assemble sliding clamps on DNA at primed sites. The τ subunit of the clamp loader connects the leading and lagging strand polymerases. SSB (orange) prevents secondary structure formation of single-stranded DNA. This figure was based on (2).

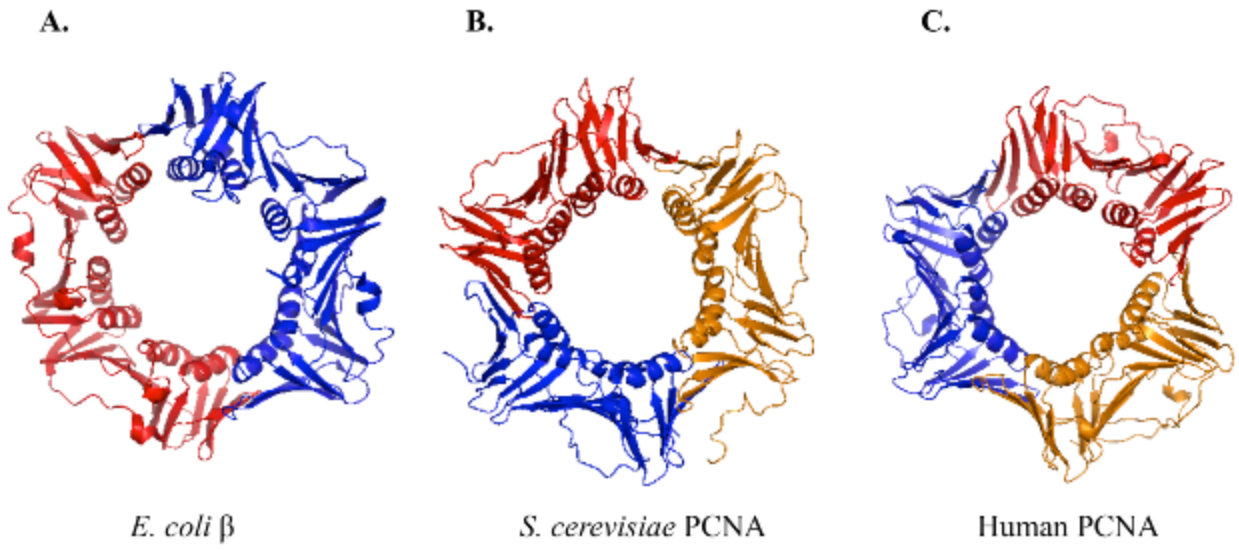

Figure 1-2. Structure of sliding clamps. Ribbon diagrams of the *E. coli* β (A), *S. cerevisiae* PCNA (B), and human PCNA (C) sliding clamps, with each subunit represented in a different color. All clamps are composed of six globular domains with comparable fold that are linked by interdomain connecting loops. Structures were generated using PDB files 2POL (13), 1SXJ (33), and 1AXC (32) for β, yeast PCNA, and human PCNA, respectively.

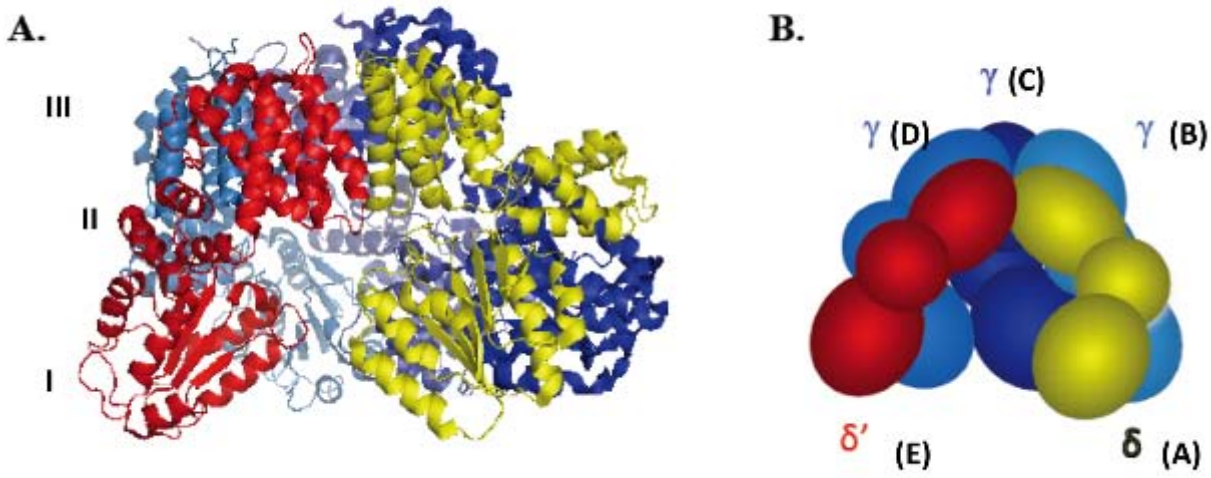

Figure 1-3. Structure of the *E. coli* clamp loader, γ complex. (A) A ribbon diagram with the subunit domains labeled starting with domain III at the C-terminal region and domain I at the N-terminal region and (B) a cartoon representation of the minimal *E. coli* γ complex , γ_3 (blue), δ (yellow), δ' (red) with the subunits labeled A-E based on their position. The clamp loader is a spiral shaped complex with its subunits held tightly together at the C-terminal domains to form a collar while the N-terminal domains are more loosely suspended. The structure was generated using PDB file 1XXH (45).

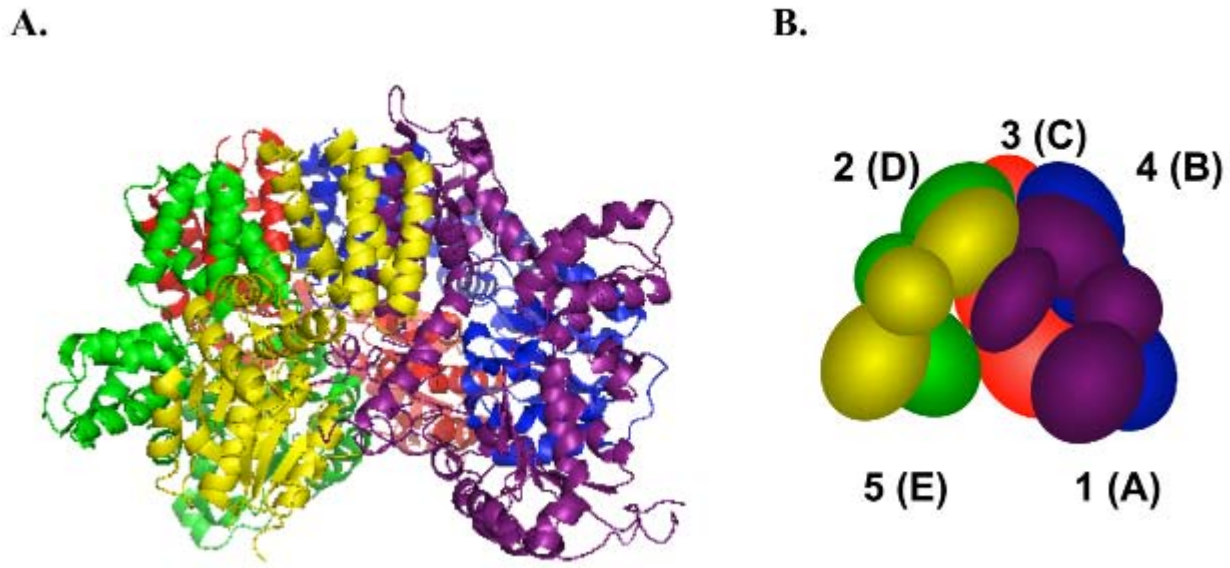

Figure 1-4. Structure of the *S. cerevisiae* clamp loader, RFC. (A) A ribbon diagram and (B) a cartoon representation of RFC with the subunits numbered and labeled A-E based on their positions. The subunits corresponding for the human RFC clamp loader are p140 (A), p40 (B), p36 (C), p37 (D), and p38 (E). RFC has similar structure and function to the *E. coli* clamp loader. The structure was generated using PDB file 1SXJ (33).

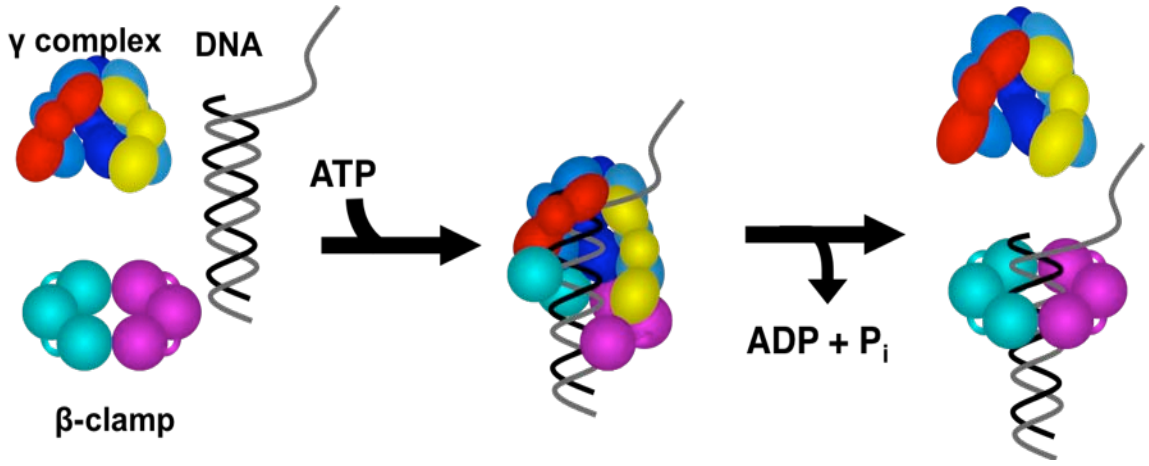

Figure 1-6 The ATP-dependent steps of the clamp loading reaction. In the first phase of clamp loading, formation of a ternary clamp loader–clamp–DNA complex is promoted by ATP binding. In the second phase, DNA binding triggers hydrolysis of ATP, the release of the clamp on DNA, and the dissociation of the clamp loader from the complex.

CHAPTER 2
MATERIALS AND METHODS

Materials

Nucleotides and Oligonucleotides

Concentrations of ATP (Amersham Biosciences/GE Healthcare) diluted with 20 mM Tris-HCl (pH 7.5) and ATPγS (Roche Diagnostics) diluted with water (Roche Diagnostics) were determined by measuring the absorbance at 259 nm and using an extinction coefficient of 15,400 $M^{-1}cm^{-1}$. Synthetic oligonucleotides were obtained from Integrated DNA Technologies (Coralville, IA) and purified by 12% denaturing polyacrylamide gel electrophoresis (PAGE). The sequences of the 60-nucleotide template and the complementary 30-nucleotide primer are as follows: 5'-TTC AGG TCA GAA GGG TTC TAT CTC TGT TGG CCA GAA TGT CCC TTT TAT TAC TGG TCG TGT-3' and 5'-ACA CGA CCA GTA ATA AAA GGG ACA TTC (C6dT) GG-3' where C6dT is a T with a C6 amino linker which was covalently labeled with 7-diethylaminocoumarin-3-carboxylic acid succinimidyl ester (Invitrogen) as described (61,73). Primed templates were annealed by incubating the 30-nucleotide primer with the 60-nucleotide template in 20 mM Tris-HCl (pH 7.5) and 50 mM NaCl at 85˚C for 5 minutes and then allowing the solution to slowly cool to room temperature. For all assays, the molar ratios of primer to template were 1:1.2 in annealing reactions.

RFC and Rad24-RFC Purification

These proteins were provided by the O'Donnell lab.

Buffers

Assay buffer used to study the *E. coli* DNA replication system contained 20 mM Tris-HCl (pH 7.5), 50 mM NaCl, and 8 mM $MgCl_2$ with the addition of 4% glycerol where

indicated. Assay buffer used to study the *S. cerevisiae* DNA replication system contained 30 mM HEPES-NaOH (pH 7.5), 150 mM NaCl, and 8 mM $MgCl_2$. *E. coli* proteins were stored in Buffer A (20 mM Tris-HCl (pH 7.5), 0.5 mM EDTA, 2 mM DTT and 10% glycerol) and γ complex storage buffer also contained 50 mM NaCl. The *S. cerevisiae* proteins were stored in 30 mM HEPES-NaOH (pH 7.5), 0.5 mM EDTA, 150 mM NaCl, 2 mM DTT, and 10% glycerol.

Methods

Purification of DNA Polymerase III Proteins

Clamp loader subunits, γ (77), δ (78), δ' (78), and χψ (55) were purified and γ complex ($\gamma_3\delta\delta'\chi\psi$) was reconstituted (48) as previously described with minor modifications as described (supplementary online material (79)).

β-Sliding Clamp Mutagenesis

Site-directed mutagenesis was performed to change the Glu-299 to Cys in a β construct in which surface cysteines 260 and 333 were replaced with serine so that Cys-299 could be selectively labeled. The QuikChange mutagenesis kit (Stratagene) was used as directed by the manufacturer for site-directed mutagenesis with the following primers (and the complementary strands): Q299C, 5' CAC CGC CAA CAA CCC GGA ATG CGA AGA AGC GGA AGA GAT C; C260S, 5' CAT CTG GAA GCT GGC TCA GAT CTG CTC AAG CAG GCG; C333S, 5' CTG AAC GCG CTG AAA CTG AGA ACG TCC GCA TGA TGC.

β-Sliding Clamp Transformation

Transformation was done by thawing 50 μL of *E. coli* BL21 (DE3) competent cells on ice and adding 10 ng of the β-Q299C mutant plasmid to the competent cells. The cells were chilled on ice for 5 min followed by heating at 42°C for 45 s and finally chilled

on ice again for 2 min. The transformed mixture was then added to 1 mL LB media and then allowed to recover in the shaker at 37°C, 250 rpm, for 1 h. A 1:10 dilution of the recovered culture was prepared by adding 100 µL culture into 900 µL of LB media. Cells were plated (100 µL of 1:1 diluted culture and 100 µL of the 1:10 diluted culture) on separate LB agar containing 100 µg/mL ampicillin. The plates were incubated at 37°C overnight for no more than 16 h. A starter culture was created by inoculating 2, 50 mL flasks containing 10 mL of LB media and 100 µg/mL ampicillin with one colony (per culture flask) from the overnight transformation. The cultures were incubated in the shaker at 37° C, 250 rpm, for 4 to 5 h and the flasks were stored at 4°C overnight.

The starter culture was aliquoted into 4, 2 mL tubes and spun at 6,000 RCF for 10 min. The supernatant was decanted and each pellet was resuspended in 500 µL of LB media with 100 µg/mL of ampicillin. Four, 2.8 L flasks were inoculated (with 500 mL of LB media with 100 µg/mL of ampicillin) with the resuspended pellets. Cultures were incubated in the shaker at 37°C, 250 rpm, until the OD_{600} reached around 0.6 to 0.7 (3 to 4 h). Expression was induced by the addition of IPTG to 1 mM, which is equivalent to adding 500 µL of 1 M IPTG per flask. The incubation was continued in the shaker at 37°C for 4 h. Cultures were chilled on ice to slow expression and then spun at 5,000 RCF at 4°C for 30 min. Pellets were decanted from the supernatant, weighed, and stored at -80°C. Samples of pre and post induction at different time points were saved to run SDS PAGE later.

β-Sliding Clamp Purification

The mutated β construct was purified (80) as previously described with the additional modifications as described (79). The pellets were thawed on ice and resuspended in 30 to 40 mL lysis buffer (20 mM Tris-HCl (pH 7.5), 0.5mM EDTA, 50

mM NaCl, and 2 mM DTT). The resuspended pellets were pressed two times in a French Press at 1,000 psi on the gauge and approximately 17,000 psi in the cell. The lysate was cleared by centrifugation at 10,000 RCF, 4 °C for 45 min. The cleared lysate/supernatant, where β is found, was decanted from the pellet. Samples of the pellet and lysate were saved to run SDS PAGE later.

All remaining purification steps are carried out at 4°C unless otherwise noted. Ammonium sulfate (0.194 g/mL, 35% saturation) was added to the clarified cell lysate. The precipitate was removed by centrifugation at 31,000 RCF for 30 min and discarded. Additional ammonium sulfate (0.218 g/mL, 70% saturation) was added to the supernatant, and the precipitate was recovered by centrifugation at 9,800 RCF for 20 min. The pellet was resuspended in Buffer A and dialyzed against Buffer A. The dialyzed protein was loaded onto two 5-mL HiTrap Q-Sepharose columns (GE Healthcare) equilibrated in Buffer A and joined in tandem. After loading, the columns were washed with 3 column volumes (30 mL) of Buffer A, and eluted with a linear gradient of 0 to 500 mM NaCl. Fractions containing a peak eluting at about 225 mM NaCl were pooled and dialyzed against 10 mM sodium acetate (pH 7.5) and 0.5 mM EDTA. Dialyzed protein was loaded onto two 5-mL HiTrap Heparin-Sepharose columns (GE Healthcare) equilibrated in 10 mM sodium acetate (pH 7.5) and 0.5 mM EDTA and joined in tandem. The material that was not retained on the column was collected and adjusted to pH 6.0 with acetic acid before loading onto the same two 5-mL HiTrap Heparin-Sepharose columns joined in tandem and equilibrated in 10 mM sodium acetate (pH 6.0) and 0.5 mM EDTA. The column was washed with 3 column volumes (30 mL) of the equilibration buffer and eluted with a linear gradient of 0 – 500 mM NaCl

over 10 column volumes. Fractions containing β eluting at about 240 mM NaCl were pooled, dialyzed against Buffer A that did not contain DTT, aliquoted, and stored at -80 °C. The total protein yield was 73.5 mg/L and had a final concentration of 4.76 mg/mL.

Covalent Labeling of the β-clamp with Pyrene

The β-Q299C mutant was labeled as described (81). The mutant protein was dialyzed against 1 L of 50 mM K_2PO_4 (pH 7.4) overnight at 4 °C and for another 5 h after β was transferred into 1 L of fresh 50 mM K_2PO_4 (pH 7.4). The N- (1-pyrene) maleimide (Molecular Probes) was dissolved in DMSO. After the addition of β, the final concentration of DMSO was 8% in solution. For the labeling reaction, the β-clamp was incubated with a 10-fold excess of pyrene (53 nmol of β monomer and 560 nmol pyrene). The β-Q299C mutant and the pyrene in DMSO solution were warmed at 37°C for 5 minutes before adding the pyrene solution to β and incubating for 2.5 h at room temperature in the dark and then stored overnight at 4°C.

The β-Q299C mutant was purified as described (72,82) using a BioRad P6-DG desalting column with buffer containing 20 mM Tris-HCl (pH 7.5) and 0.5 mM EDTA to remove excess free dye from the labeled β-PY. Fractions containing β-PY were then loaded onto a 1 mL HiTrap Q-Sepharose anion exchange column (GE Healthcare) equilibrated with Buffer A and washed for 10 column volumes (10 mL) to remove excess pyrene noncovalently bound. The protein was eluted with Buffer A containing 0.5 M NaCl. The β-PY was dialyzed against Buffer A that did not contain DTT, aliquoted, and stored at -80 °C.

PCNA Sliding Clamp Mutagenesis

Site-directed mutagenesis was performed to change the Ile-111 and Ile-181 to Cys in a PCNA construct in which surface cysteines 22, 62, and 81 were replaced with

serine so that Cys-111 and Cys-181 could be selectively labeled. The QuikChange mutagenesis kit (Stratagene) was used for site-directed mutagenesis as per the manufacturers instructions with the following primers (and the complementary strands): I111C, 5’ GGA TAC CAG AAA GAC CGT TGT GCC GAA TAC TCT CTG; I181C, 5’ CGG ATC AGG TTC AGT CTG TAT AAA ACC ATT CGT GG; C22S, 5’ GGA AAT TGA CCA ACT GGA CGG AAT CTT TGA AAC CAT C; C62S, 5’ CCT AAC GTA ACA GGA TGG TCG GAT CTA TAT TCT TGG AAG GC; C81S, 5’ GTA TCG GTG TTG TTA CCG GAA CGT AGG ATT TTA CTT AG.

PCNA Sliding Clamp Transformation

The mutant PCNA was purified based on a protocol previously described (83) with the additional modifications as described. Transformation was done by thawing 50 µL of *E. coli* BL21 (DE3) competent cells on ice and adding 10 ng of PCNA-I111C/I181C mutant plasmid to the competent cells. The cells were chilled on ice for 5 min followed by heating at 42°C for 45 s and finally chilled on ice again for 2 min. The transformed mixture was then added to 1 mL LB media and then allowed to recover in the shaker at 37°C, 250 rpm, for 1 h. A 1:10 dilution of the recovered culture was prepared by adding 100 µL culture into 900 µL of LB media. Cells were plated (100 µL of 1:1 diluted culture and 100 µL of the 1:10 diluted culture) on separate LB agar containing 100 µg/mL of ampicillin. The plates were incubated at 37°C, overnight for no more than 16 h. A starter culture was created by inoculating 2, 50 mL flasks containing 10 mL of LB media and 100 µg/mL of ampicillin with one colony (per culture flask) from the overnight transformation. The cultures were incubated in the shaker at 37° C, 250 rpm, for 4 to 5 h and the flasks were stored at 4°C overnight.

The starter culture was aliquoted into 4, 2 mL tubes and spun at 6,000 RCF for 10 min. The supernatant was decanted and each pellet was resuspended in 500 µL of LB media with 100 µg/mL of ampicillin. Four, 2.8 L flasks were inoculated (with 500 mL of LB media with 100 µg/mL of ampicillin) with the resuspended pellets. Cultures were incubated in the shaker at 37°C, 250 rpm, until the OD_{600} reached around 0.6 to 0.7 (3 to 4 h). Expression was induced by the addition of IPTG to 1 mM, which is equivalent to adding 500 µL of 1 M IPTG per flask. The incubation was continued in the shaker at 37°C for 4 h. Cultures were then chilled on ice to slow expression and then spun at 5,000 RCF at 4°C for 30 min. Cell pellets were decanted from the supernatant, weighed, and stored at -80°C. Samples of pre and post induction at different time points were saved to run SDS PAGE later.

PCNA Sliding Clamp Purification

The cell pellets were thawed on ice and resuspended in 30 to 40 mL lysis buffer (20 mM Tris-HCl (pH 7.5), 0.5mM EDTA, 50 mM NaCl, and 2 mM DTT). The resuspended pellets were pressed two times in a French Press at 1,000 psi on the gauge and approximately 17,000 psi in the cell. The lysate was cleared by centrifugation at 10,000 RCF, 4 °C for 45 min. The cleared lysate/supernatant, where PCNA is found, was decanted from the pellet. Samples of the pellet and lysate were saved to run SDS PAGE later.

All remaining purification steps are carried out at 4°C unless otherwise noted. The volume of the cleared lysate was adjusted to 50 mL with Buffer A containing 50mM NaCl and ammonium sulfate (0.2 g/mL, 40% saturation) was slowly added to the clarified lysate over 30 min with gentle stirring. The precipitation continued for about 1.5 h after the final addition of ammonium sulfate. The precipitate was removed by

centrifugation at 31,000 RCF at 4 °C for 30 min and discarded. The recovered supernatant volume was determined and then multiplied by 0.15 g/mL (60% saturation). Ammonium sulfate was slowly added over 1 h and allowed to continue precipitation for 1.5 h after the final addition. The precipitate was removed by centrifugation at 31,000 RCF at 4 °C for 30 min and discarded. The recovered supernatant volume was determined and then multiplied by 0.15 g/mL (85% saturation). Ammonium sulfate was slowly added over 1.5 h and allowed to continue precipitation for 1 h after the final addition. The precipitate was recovered by centrifugation at 9,800 RCF for 25 min at 4 °C. PCNA is not in the supernatant but in the pellet. The pellet was resuspended in about 10 mL Buffer A containing 50 mM NaCl and then the resuspension was dialyzed against 2 L Buffer A containing 50 mM NaCl overnight using SpectraPor 2 (Spectrum Laboratories) dialysis membrane with a molecular weight cutoff of 12,000 to 14,000 g/mol. PCNA was placed into fresh dialysis buffer (2 L Buffer A containing 50 mM NaCl) and dialyzed for another 5 to 6 h.

Two 5 mL HiTrap Q-Sepharose columns (GE Healthcare) were equilibrated with Buffer A containing 50 mM NaCl. The recovered PCNA solution from dialysis was loaded onto the column via a peristaltic pump at a rate of 2 mL/min and the flow through was collected. The column was washed with 50 mL Buffer A containing 50 mM NaCl. A linear gradient was run from 50 mM to 700 mM NaCl over 150 mL at 2.5 mL/min and 1.8 mL fractions were collected. PCNA is expected to elute at approximately 450 mM NaCl. To confirm presence of PCNA, SDS PAGE was run on the fractions to be pooled. The pooled fractions were dialyzed overnight against 2 L of 25 mM KPO_4 (pH 7.0), 2 mM DTT, and 10% glycerol in a SpectraPor 2 membrane with a molecular weight cutoff

of 12,000-14,000 g/mol. PCNA was put into fresh dialysis buffer at least one time and dialyzed for another 5 to 6 h.

A 5 mL HiTrap SP-Sepharose column (GE Healthcare) was equilibrated with 25 mM KPO_4 (pH 7.0), 2 mM DTT, and 10% glycerol. The recovered PCNA solution loaded onto the column via a peristaltic pump at 2 mL/min. The PCNA will flow through this column. An 8 mL MonoQ column (GE Healthcare) equilibrated with 25 mM KPO_4 (pH 7.0), 2 mM DTT, and 10% glycerol. Inject the PCNA collected from the SP-Sehparose column flow through via a large injecting loop. Wash the column with 40 mL of 25 mM KPO_4 (pH 7.0), 2 mM DTT, and 10% glycerol. Run a linear gradient from 0 to 700 mM KCl over 80 mL at 2 mL/min and collect 1 mL fractions. PCNA is expected to peak at approximately 420 mM KCl. To confirm presence of PCNA, run SDS PAGE of the fractions to be pooled. Dialyze the pooled fractions overnight against 2 L of 30 mM HEPES-NaOH (pH 7.5), 150 mM NaCl, 2 mM DTT, and 10% glycerol in a SpectraPor 2 membrane with a molecular weight cutoff of 12,000-14,000 g/mol. Change to fresh dialysis buffer at least one time and dialyze for another 5 to 6 h. Aliquot the PCNA and store at -80°C. The total protein yield was 20.5 mg/L and had a final concentration of 5.94 mg/mL determined by measuring the absorbance at 280 nm in 6 M guanidine hydrochloride and using the calculated extinction coefficient 6,170 M^{-1} cm^{-1} for PCNA.

Covalent Labeling of the PCNA-clamp with AlexaFluor 488

For the labeling reaction, a solution of 50 mM TCEP in 0.2 M Tris base (pH 8.0) is added to PCNA and allowed to sit for 5 min. TCEP would reduce any disulfide bond formation that may occur between the cysteine residues. The AlexaFluor 488 C_5 maleimide (AF488) (Molecular Probes) was dissolved in DMSO. After the addition of the PCNA-I111C/I181C solution, the final concentration of DMSO was 8%. The PCNA

solution is incubated with a 30-fold excess of AF488, (65 nmol of PCNA and 1.9 μmol of AF488). The AF488 in DMSO solution was added to PCNA and incubated for 4 h at room temperature in the dark.

The AF488-labeled PCNA was purified using a BioRad P6-DG desalting column with buffer containing 30 mM HEPES-NaOH (pH 7.5), 150 mM NaCl, and 0.5 mM EDTA to remove excess free dye. One mL fractions were collected and pooled. Fractions containing PCNA-AF488, which eluted in the void volume, were combined and loaded onto a 1 mL HiTrap Q-Sepharose anion exchange column (GE Heathcare) equilibrated with 30 mM HEPES-NaOH (pH 7.5), 150 mM NaCl, 0.5 mM EDTA, and 10% glycerol. The loaded protein was washed for 10 mL with 30 mM HEPES-NaOH (pH 7.5), 150 mM NaCl, 0.5 mM EDTA, and 10% glycerol to remove excess AF488 and then eluted with 30 mM HEPES-NaOH (pH 7.5), 150 mM NaCl, 0.5 mM EDTA, and 10% glycerol containing 0.5 M NaCl. The PCNA-AF488 was dialyzed against 30 mM HEPES-NaOH (pH 7.5), 150 mM NaCl, 0.5 mM EDTA, 2 mM DTT, and 10% glycerol, aliquoted, and stored at -80 °C.

Protein Concentrations

Concentrations of γ complex were determined by measuring the absorbance at 280 nm in 6 M guanidine hydrochloride and using the calculated extinction coefficient (220,050 $M^{-1}cm^{-1}$). The protein concentration of β-PY was determined using the Modified Lowry Protein Assay using bovine serum albumin (BSA) as standards (Pierce). Based on the concentration of protein and the concentration of pyrene determined by its absorbance at 338nm (extinction coefficient of 40,000 M^{-1} cm^{-1}), the typical labeling efficiency was 60%. The concentrations of RFC and PCNA were determined my measuring the protein absorbance at 280 nm in 6 M guanidine hydrochloride and using

the calculated extinction coefficient 162,120 M^{-1} $cm^{-1}$and 6,170 M^{-1} cm^{-1}, for RFC and PCNA, respectively.

Labeling Primer DNA with DCC

The 12% PAGE purified 30-nucleotide primer was covalently labeled with a 20-fold excess of DCC overnight at room temperature. The DCC-labeled primer DNA was extracted using chloroform and concentrated BuOH then run on a desalting column containing rehydrated BioRad P6-DG resin with 20 mM Tris-HCl (pH7.5) and 0.5 mM EDTA to remove excess free dye. To remove unlabeled oligonucleotides from the labeled oligonucleotides, the DCC-labeled DNA was purified by 12 % PAGE, eluted in a sterile buffer of NaCl, Tris, and EDTA and stored at -20 °C.

Experimental Procedures

Steady State Fluorescence Assays

Fluorescence emission spectra were measured using a QuantaMaster QM-1 fluorometer (Photon Technology International) or an Edinburgh Analytical Instruments FS900 fluorometer. DCC-labeled DNA was excited at 440 nm and emission scanned from 450 to 550 nm using a 3.6-nm bandpass on the Edinburgh SF900 fluorometer. PY-labeled β was excited at 345 nm and emission scanned from 355 to 455 nm using a 5-nm bandpass on the Photon Technology International fluorometer. Equilibrium binding of γ complex to β-PY was done by adding reagents sequentially to the cuvette starting with 72 µL of assay buffer with ATP, followed by 4 µL of β-PY, and finally 4 µL of γ complex for a total reaction volume of 80 µL. Stoichiometric binding of γ complex to β-PY or DNA-DCC was done by adding reagents sequentially to the cuvette starting with 68 µL of assay buffer, followed by 4 µL of β-PY or p/t-DNA-DCC, 4 µL of γ complex, and finally 4 µL of ATP (or ATPγS for DNA) for a total reaction volume of 80 µL. For both

equilibrium and stoichiometric β-PY binding assays, emission spectra were measured following each addition, and intensities relative to free β-PY at 375 nm were plotted as a function of γ complex concentration.

PCNA-AF488 was excited at 495 nm and emission scanned from 505 to 605 nm using a 2.5-nm bandpass on the Photon Technology International fluorometer. Equilibrium binding of RFC or Rad24-RFC to PCNA-AF488 was done by adding reagents sequentially to the cuvette starting with 72 µL of assay buffer with ATP, followed by 4 µL of PCNA-AF488, and finally 4 µL of RFC or Rad24-RFC for a total reaction volume of 80 µL. Emission spectra were measured following each addition and relative intensities at 518 nm were plotted as a function of RFC concentration.

Pre-Steady State Fluorescence Assays

Assays were done using an Applied Photophysics SX20MV stopped-flow apparatus at 20˚C. Single-mix reactions were performed by mixing equal volumes (50 µL) of reagents immediately before they entered the cuvette. Data were collected for a total of 5 s at intervals of 1 ms. Final concentrations for each experiment in assay buffer with 4% glycerol are indicated in the *Figure Legends* and/or *Results*. Measurements of DCC fluorescence were made using a 455-nm cut-on filter to collect emission while exciting at 430 nm with a 3.72-nm bandpass. A 365-nm cut-on filter was used to collect PY emission when exciting at 345-nm using a 3.72-nm bandpass for β^{PY} binding experiments.

Data Analysis

Steady State Fluorescence Assays

Emission spectra were corrected for background by subtracting the signal for free PY, DCC, or AF488 signal during analysis. The dissociation constant (K_D) of the β-PY•γ

complex was calculated by fitting the observed intensity data (I_{obs}) to equation 1 in which γ_c is the concentration of γ complex, β is the concentration of β-PY, I_{min} is the intensity of free β-PY and I_{min} is the intensity of γ□complex•β-PY. The intensity of γ□complex•β-PY (I_{max}) and K_D were fit as adjustable parameters by nonlinear regression using KaleidaGraph.

$$I_{obs} = \frac{(K_D + \gamma_c + \beta) - \sqrt{(K_D + \gamma_c + \beta)^2 - 4\gamma_c\beta}}{2\beta}(I_{\max} - I_{\min}) + I_{\min} \qquad (2\text{-}1)$$

Equation 2-1 was also used to fit the quench in DCC fluorescence as a function of γ complex in the DNA binding assay to calculate the relative intensity of a clamp loader•DNA complex and a K_D value. In this case, the concentration of DNA was substituted for β, I_{max} represents the intensity of free DNA, and I_{min} represents the intensity of bound DNA.

Equation 2-1 was also used to fit the quench in AF488 fluorescence as a function of RFC in the PCNA opening assay to calculate the relative intensity of a clamp loader•clamp complex and a K_D value. In this case, the concentration of PCNA was substituted for β, I_{min} represents the intensity of free PCNA-AF488, and I_{max} represents the intensity of bound RFC•PCNA-AF488.

Pre-Steady State Fluorescence Assays

Time courses for β-PY binding were empirically fit to a single exponential rise, $y = a(1\text{-}e^{-kobs \cdot t}) + c$, using KaleidaGraph to determine values for observed rate constants, k_{obs}, as a function of γ complex concentration.

Kinetic Modeling

DNA binding data in Fig. 3-6, 3-8, and 3-10 were globally fit to the model illustrated in Fig. 3-11 using DynaFit to calculate the rate constants given in the figure. All of the

rate constants were treated as adjustable parameters; none were set at fixed values. The relative intensity for free DNA and for the initial clamp loader•DNA complex prior to the DNA-induced conformational change were set to 1, and the relative intensities for all other clamp loader•DNA complexes were set to the value of 0.58 derived from the titration in Fig. 3-7B. Concentrations of protein and DNA were fixed based on the concentrations determined experimentally from absorbances at 280 nm and 260 nm, respectively, as described above. In experiments in which γ complex was pre-incubated with ATP, the "incubate" and "dilute" functions in DynaFit were used to generate the equilibrium concentrations of the two conformational states of γ complex that exist in the presence of ATP (84). These functions were used to: 1) mix a solution of γ complex, twice as concentrated as in the final reaction, with ATP, 2) dilute γ complex in half to the final concentration, and 3) incubate the solution for 1 s *in silico* to generate the equilibrium populations of conformational states that is added to DNA to initiate the binding reactions. In experiments in which γ complex was not pre-incubated with ATP, reactions were initiated *in silico* by adding free γ complex to ATP and DNA.

CHAPTER 3
RESULTS

Introduction

In the presence of ATP, γ complex binds with high affinity to β and DNA to form a ternary complex. Binding to primed template DNA triggers the clamp loader to hydrolyze all three molecules of ATP (84-86). Upon ATP hydrolysis, β is released onto DNA and the clamp loader dissociates from the β•DNA complex. Thus the clamp loading reaction can be divided into two stages based on ATP requirements: 1) formation of a ternary complex requiring ATP binding, and 2) dissociation of the ternary complex to load β on DNA requiring ATP hydrolysis. This work focuses on steps in the first phase involving the formation of the ternary complex (81).

High affinity binding of the clamp loader to the β-clamp and to DNA requires ATP binding by the clamp loader (27,73,74). Presumably, ATP binding promotes conformational changes within the clamp loader that expose surfaces/residues that interact with the clamp and DNA. When equilibrated with ATP, γ complex can bind either the clamp or DNA; however, a productive clamp loading reaction most likely requires the clamp loader to bind the clamp before binding DNA. When γ complex alone binds p/t-DNA, the interaction with DNA triggers rapid ATP hydrolysis and dissociation of the clamp loader (75,76). Therefore, clamp loading would be more efficient if there were some mechanism to favor clamp binding before DNA binding and productive clamp loading. One such mechanism would be a kinetic preference for the clamp loader to bind the clamp before DNA. This kinetic preference could be established simply by the clamp loader binding the clamp at a faster rate than DNA. Alternatively, given that the clamp loader has three ATP binding sites, sequential filling

of ATP sites and incremental conformational changes could allow the clamp loader to bind the clamp before DNA. In other words, a subset of sites bind ATP and induce conformational changes that promote β binding faster than the subset of sites that bind ATP and make conformational changes to promote DNA binding. In this work, the questions of whether there is a kinetic preference for γ complex to bind β prior to DNA and how the overall rates of ATP-induced conformational changes contribute to the rates of clamp and DNA binding are addressed.

Equilibrium Binding of γ complex to β

The clamp loader when charged with ATP has a high affinity for the clamp. The equilibrium dissociation constant (K_D) of γ complex•β is in the low nanomolar range (27). In previous studies, an anisotropy assay was used to measure γ complex•β binding (61,72), but a limitation of this assay is that it is not sensitive enough to work at low nanomolar protein concentrations, where K_D values are accurately determined. Therefore, a more sensitive intensity-based fluorescence assay was developed to measure clamp loader•clamp binding. In this assay, the Gln-299 in β was mutated to Cys, and Cys-299 was covalently labeled with pyrene (PY). Based on available structural data and similarities between the *E. coli* and yeast clamps and clamp loaders (33,34,45), residue 299 in β is likely to be near a site where a γ subunit contacts the surface of the β-clamp in a clamp loader•clamp complex (Fig. 3-1). Given the head-to-tail symmetry of the β dimer and the anticipated contacts between γ complex and β, the fluorescence of PY is likely to be affected by γ complex binding only at the position near the middle γ subunit (Fig. 3-1). Although there are two fluorophores per β-clamp (one on each monomer), γ complex will likely only interact with one monomer at time. When γ complex binds to β-PY, PY fluorescence increases (Fig. 3-2). At saturating

concentrations of γ complex, the intensity of PY is just over two and a half times greater than for free β-PY (81).

This increase in PY fluorescence was used to measure equilibrium binding of γ complex to β-PY and calculate the dissociation constant for the interaction. A K_D value of 5.0 ± 2.4 nM was calculated from three independent experiments at 10 nM β-PY (average values are shown in Fig. 3-3A). This K_D value is in agreement with the value of 3.2 nM previously reported (27). Binding was measured at a higher concentration of β-PY (80 nM) to determine the dissociation constant for the weaker ATP-independent binding reaction (Fig. 3-3B, filled circles) and to determine the stoichiometry of binding in the presence of ATP (Fig. 3-3B, filled squares). The K_D value calculated for ATP-independent binding was 135 ± 32 nM, which is in agreement with the value 151 nM reported previously (72). In the presence of ATP, γ complex binds β with the expected 1:1 stoichiometry as indicated by achieving saturation at a concentration of around 80 nM γ complex, and these data also give a calculated K_D value of 2.9 nM for ATP-dependent binding. Interestingly, the maximum increase in PY fluorescence in assays without ATP is less than 2-fold, whereas it is greater than 2.5-fold in the presence of ATP. This difference could reflect differences in conformational states of γ complex and/or β in the presence and absence of ATP. ATP is shown to cause a conformational change in γ complex that gives it a high affinity for the clamp (27). The clamp is likely to be open in clamp loader-clamp complexes in assays with ATP, whereas it is likely to be closed in clamp loader-clamp complexes in assays without ATP (60).

Kinetics of γ complex binding β

To determine the rate of γ complex binding β, the increase in PY intensity was measured in real time when a solution of γ complex and ATP was mixed with a solution

of β-PY and ATP. Reactions contained 20 nM β-PY and γ complex concentrations of 10, 20, 40, and 80 nM (Fig. 3-4A). These time courses were empirically fit to exponential rises to calculate apparent rate constants, k_{obs}. These k_{obs} values were plotted as a function of γ complex concentration and fit to line to calculate an apparent on-rate constant, $k_{on, app}$, of 2.3 x 10^7 M^{-1} s^{-1} and an apparent dissociation rate constant, $k_{off, app}$, of 0.14 s^{-1} from the slope and y-intercept, respectively (87) (Fig. 3-4B). The apparent K_D value calculated from these kinetic constants was 6 nM, which is in agreement with the value determined from equilibrium measurements.

Binding of γ complex to DNA

A fluorescence intensity-based assay was used in which the primer strand of p/t-DNA is labeled with DCC three nucleotides from the 3' end, p/t-DNA-DCC, was used to measure the kinetics of γ complex binding to DNA (61). When the clamp loader binds DNA at the primer/ template junction, the environment of DCC is altered and the fluorescence decreases. The γ complex requires ATP binding for high affinity binding to DNA, but DNA binding triggers hydrolysis of ATP and dissociation of the clamp loader so that binding is transient (75,88). Therefore, γ complex•DNA binding under equilibrium conditions was measured in assays with the non-hydrolyzable ATP analog, ATPγS. When γ complex binds p/t-DNA-DCC, the fluorescence is quenched and the emission maximum of DCC is blue-shifted by 5 to 6nm (Fig. 3-5A). To determine the magnitude of the fluorescence quench and relative quantum yield of a clamp loader•DNA complex, p/t- DNA-DCC was titrated with γ complex in the presence of ATPγS (Fig. 3-5B). These titration data showed that the fluorescence of the protein•DNA complex is 58% of the fluorescence of free p/t-DNA-DCC.

Transient binding of γ complex to DNA in assays with ATP was measured in real time stopped-flow fluorescence experiments. A solution of γ complex and ATP was added to a solution of p/t-DNA-DCC and ATP, and the intensity of DCC was measured as a function of time (Fig. 3-6). Binding rates were measured with increasing concentrations of γ complex and DNA at 125, 250, and 500 nM. In each case, a rapid decrease in DCC fluorescence due to γ complex binding p/t-DNA-DCC was followed by a rapid increase in fluorescence due to dissociation of γ complex from DNA following ATP hydrolysis. As the concentrations of γ complex and DNA were increased, the binding reaction became faster and the magnitude of the fluorescence quench increased. However, the magnitude of the decrease in fluorescence at the lowest point was not as large as measured in assays with ATPγS (Fig. 3-5B). Moreover, these reactions are not approaching a limiting value for the minimum fluorescence, but continue to decrease with increasing concentrations. Assuming that the magnitude of the quench in fluorescence is the same for clamp loader•DNA complexes in assays with ATP and ATPγS, this shows that the ATP hydrolysis-induced γ complex dissociation is fast relative to the DNA binding reaction so that only a fraction of p/t-DNA-DCC is bound when the fluorescence reaches a minimal value. Given a relative fluorescence of 58% for the clamp loader•DNA complex, about 14% of the p/t-DNA-DCC is bound when the intensity reaches a minimum value of about 0.94 in the reaction containing 500 nM γ complex and p/t-DNA-DCC.

Rates of γ Complex Binding β with and without Preincubation of γ Complex with ATP

ATP binding promotes conformational changes in γ complex that give it a high affinity for the clamp and DNA. It is possible that the rates of these conformational

changes govern the rates of clamp and DNA binding to the clamp loader. To test this possibility, the rate of γ complex binding β^{PY} was measured in assays in which γ complex was preincubated with ATP (Fig. 3-7A, gray trace) and in which γ complex is added to ATP at the same time as β-PY (Fig. 3-7A, black trace). After mixing, both reactions contained identical concentrations of β-PY (200 nM), γ complex (200 nM), and ATP (0.5 mM). There was no difference between the binding rates when γ complex was preincubated or not with ATP before adding β. This suggests that ATP binding and ATP-induced conformational changes that give γ complex a high affinity for β are relatively rapid. When β-PY binding was measured in the absence of ATP (Fig. 3-7B, gray trace), binding was equally as rapid but a smaller fraction of β was bound than in a reaction with ATP (Fig. 3-7B, black trace). The smaller fraction bound is consistent with the weaker ATP-independent binding reaction (Fig. 3-3B). This result provides additional support that ATP binding and ATP-induced conformational changes that give γ complex a high affinity for β are relatively rapid.

DNA Binding with and without ATP Preincubation

To determine whether the rate of ATP binding and ATP-induced conformational changes could limit the rate at which γ complex binds DNA, DNA binding was measured in real time assays in which γ complex was preincubated with ATP or in which γ complex was added to ATP at the same time as p/t-DNA-DCC. When a solution of γ complex and ATP was added to a solution of p/t-DNA-DCC and ATP (ATP preincubation), a rapid quench in fluorescence occurred that reached a minimum value in about 60–70 ms and was followed by an increase in fluorescence that reached a steady state level within about 500 ms (Fig. 3-8, black trace, gray line). In contrast, when a solution of γ complex without ATP was added to a solution of p/t-DNA-DCC and

ATP (no ATP preincubation), the decrease in DCC fluorescence is slower overall (Fig. 3-8, gray trace, black line). There is a short lag of at least 25 ms before fluorescence begins to decrease and the rate of decrease is slower, such that the maximal quench occurs between 150 and 200 ms. Final concentrations of γ complex (200 nM) and pt/-DNA-DCC (200 nM) were the same in both reactions. Because the overall binding rate is slower, but the subsequent rates of ATP hydrolysis and γ complex•DNA dissociation are likely to be the same, the amplitude of the change in fluorescence is smaller when γ complex was not preincubated with ATP. This experiment was repeated with ATPγS instead of ATP to measure DNA binding in the absence of DNA-triggered ATP hydrolysis and subsequent clamp loader dissociation (Fig. 3-9). Although the reaction in which γ complex was preincubated with ATPγS was slightly faster than the non-preincubated case, overall both reactions were much slower and took 6–8 s to reach completion. It is possible that DNA binding reactions are slower in assays with ATPγS because ATPγS does not have the efficacy of ATP in promoting conformational changes that allow the clamp loader to bind DNA. We have also observed a decrease in the affinity of γ complex for β in assays with ATPγS compared with ATP (61). For this reason, we chose to focus on assays with ATP even though the kinetics are complicated by hydrolysis. In any case, a slow ATP-dependent step is bypassed when γ complex is preincubated with ATP.

Effect of ATP Concentration on γ Complex•DNA Binding Kinetics

Either a slow ATP binding step or a slow ATP-induced conformational change could limit the rate at which γ complex binds DNA. To determine which step is slow, rates of γ complex•DNA binding were measured as a function of ATP concentration in reactions in which γ complex was not preincubated with ATP. A solution of γ complex

and p/t-DNA-DCC was mixed with solutions of ATP, and DCC fluorescence was measured as a function of time. In Fig. 3-10, reactions containing 25 (A, red), 50 (B, green), 250 (C, orange), and 500 μM (D, blue) ATP are plotted in the same graph with a plot of a reaction containing 100 μM ATP (black trace). At the lowest concentration of ATP used, the reactions approached a maximal rate, becoming slightly faster with increasing concentrations of ATP, and reaching a maximum rate at 100 μM ATP. In all previous experiments, reactions contained 500 μM ATP, therefore, ATP binding was unlikely to be rate-limiting. The slower rates of DNA binding in assays in which γ complex was not preincubated with ATP must be due to a slow ATP-induced conformational change.

Kinetic Modeling of DNA Binding Reactions

DNA binding data were modeled to get an estimate of the rate of the ATP-induced conformational change that precedes DNA binding to determine whether there could be a kinetic preference for binding β prior to DNA. A kinetic model from previous studies was adapted to fit these DNA binding data (84). The kinetic model was developed based on experiments measuring rates of ATP hydrolysis in reactions in which γ complex was preincubated with ATP for varying periods of time before adding p/t-DNA. The earlier studies revealed that the rate of ATP hydrolysis was limited by an ATP-dependent conformational change and suggested that a slow ATP-induced conformational change activates the clamp loader for DNA binding. Experiments in Figs. 3-8 and 3-10 confirm this by establishing that a slow ATP-induced conformational change precedes DNA binding.

The complete kinetic mechanism is quite complex and contains too many forward and reverse rate constants to define in a single set of experiments. Therefore, the

kinetic model was simplified by including only forward rates for most of the steps and allowing three molecules of ATP to bind and three molecules of ADP to dissociate as a unit in a single step. All of the rate constants shown in Fig. 3-11 were derived by globally fitting the data in Figs. 3-6, 3-8, and 3-10 to the model shown using DynaFit (89). The forward and reverse rate constants for the ATP-induced conformational change obtained from DNA binding data were 3.3 and 1.7 s^{-1} compared with values of 6.5 and 3.9 s^{-1}, respectively, obtained previously from fits of ATP hydrolysis data. After the conformational change, p/t-DNA binding occurred at a rate of 4.0 x 10^7 M^{-1} s^{-1}. The rate of DNA binding is similar to the rate of clamp binding (2.3 x 10^7 M^{-1} s^{-1}) and on the order of what would be expected for a diffusion-limited rate for two macromolecules interacting. However, in reactions in which γ complex is not preincubated with ATP, the rate of DNA binding is limited by the slow, 3.3 s^{-1} conformational change, whereas the rate of β binding is not. The interaction with p/t-DNA triggers a change in the clamp loader that makes the ATP sites competent for hydrolysis, and in the model used here, three molecules of ATP are hydrolyzed sequentially before DNA is released. ADP release allows the clamp loader to go through the cycle again.

The DNA binding data do not provide a direct measure of ATP hydrolysis, and in terms of these data, the ATP hydrolysis steps in the kinetic model provide a time lag between observed DNA binding and release. The model used to fit DNA binding data here differs from that used to fit ATP hydrolysis data in that two molecules of ATP were hydrolyzed rapidly and the third slowly in the ATP hydrolysis model. The DNA binding data could be fit equally well by a model in which ATP hydrolysis occurred in two phases (data not shown), hydrolysis of two molecules of ATP rapidly before DNA

release, and hydrolysis of one molecule of ATP slowly after DNA release as proposed previously based on ATP hydrolysis data (84). When DNA binding data were fit to this two-phase model for ATP hydrolysis, similar rates for ATP binding ($k_{on\ (ATP)}$ = 12.6 μM^{-1} s^{-1}), the ATP-induced conformational change (k_{conf} = 3.3 s^{-1}, $k_{rev\ (conf)}$ = 1.7 s^{-1}), DNA binding (3.9 x 10^7 M^{-1} s^{-1}), and DNA release (88 s^{-1}) were obtained. Therefore, for the purposes of this study, which focuses on the overall rate of DNA binding, we used the simpler model in which all three molecules were hydrolyzed at the same rate.

Discussion

Clamp loaders catalyze the assembly of sliding clamps onto DNA for use by DNA polymerases. To load clamps, the affinity of the clamp loader for the clamp and DNA must be modulated. Initially, the clamp loader must have a high affinity for the clamp and DNA to bring these macromolecules together, but then the affinity must decrease so that the clamp loader can release the clamp onto DNA. This affinity modulation is achieved by ATP binding and hydrolysis. ATP binding activates the clamp loader for binding the clamp and DNA, whereas ATP hydrolysis deactivates the clamp loader, releasing the clamp and DNA. The clamp loading reaction can be divided into two phases depending on the ATP requirements: 1) ATP binding-dependent formation of a ternary clamp loader•clamp•DNA complex, and 2) ATP hydrolysis-dependent decay of the ternary complex releasing the clamp on DNA. Much of our previous work focused on the second phase of the reaction by adding a preformed clamp loader-clamp complex to DNA to rapidly form the ternary complex via a single pathway. Here, we focused on the first phase of the reaction, formation of a ternary clamp loader-clamp complex. We asked whether γ complex binds the clamp or DNA faster, and how preincubation of the clamp loader with ATP to form the ATP-activated state affects the rates of clamp loader-

clamp and clamp loader-DNA binding.

To measure the rate of clamp binding, a sensitive fluorescence intensity-based assay was developed in which the β-clamp was covalently labeled with PY. The intensity of PY increases when the clamp loader binds the clamp. An advantage of this assay is that clamp loader-clamp binding can be measured directly in solution and in real time. The assay is sensitive enough to measure the high affinity binding of γ complex to β under equilibrium conditions as well as measuring binding kinetics on a millisecond time scale. Using this binding assay, a bimolecular rate constant of 2.3×10^7 M^{-1} s^{-1} was determined for γ complex binding β in the presence of ATP. This rapid rate indicates the binding interaction is limited by the rate of diffusion of the proteins.

Two Sets of ATP-induced Conformational Changes

High affinity binding of the clamp loader to the clamp and to DNA requires the clamp loader to bind ATP first. Presumably, ATP binding promotes conformational changes in the clamp loader that place amino acid residues and protein surfaces in the appropriate conformation to productively interact with the clamp and DNA (27,60,76). Interestingly, our results strongly suggest that a different set of ATP-induced conformational changes is required to promote binding of the clamp loader to the clamp versus binding to DNA (81) (Fig. 3-12).

Given that ATP-induced conformational changes must precede clamp or DNA binding, the overall rate of these conformational changes will contribute to observed binding rates in experiments in which γ complex is not preincubated with ATP prior to adding the clamp or DNA. On the other hand, if γ complex is preincubated with ATP before adding the clamp or DNA, these conformational changes can take place during the preincubation period and binding rates will not be influenced by the rate of the

conformational changes. When γ complex was preincubated with ATP, the rate of p/t-DNA binding was faster than for reactions in which γ complex was not allowed to bind ATP before p/t-DNA (see Fig. 3-8). DNA binding kinetics measured as a function of ATP concentration (see Fig. 3-10) demonstrated that the slower DNA binding kinetics were not due to a slow ATP binding reaction, but instead must be the result of slow ATP-induced conformational changes.

In contrast, the observed rate for β binding was the same regardless of whether γ complex was preincubated with ATP or not (see Fig. 3-7). The rapid β binding in experiments without ATP preincubation is unlikely to be due to an ATP-independent binding reaction because the ATP-independent binding interaction is weaker (see Fig. 3-3B) and could only account for a fraction of the binding events (see Fig. 3-7B). ATP binding and subsequent ATP induced conformational changes are rapid relative to the rate of β binding. Given that only DNA binding rates are limited by a slow ATP-induced conformational change, this would suggest that a different set of conformational changes gives rise to β and DNA binding (81).

A Kinetic Preference for the Clamp Loader to Bind β before DNA

When equilibrated with ATP, the *E. coli* γ complex can bind either β or DNA. The same is true for the eukaryotic clamp loader, RFC (90). Although these clamp loaders can bind either the clamp or DNA, productive clamp loading is likely to require these clamp loaders to bind the clamp first. In contrast, the bacteriophage T4 clamp loader can productively load clamps by binding either DNA or the clamp first (91,92). This may be due to differences in the solution structures of the clamps. The bacteriophage T4 gp45 clamp exists as an open ring in solution (93,94), whereas the *E. coli β* clamp (95) and eukaryotic clamp are likely to exist as closed rings in solution (96).

When bound to genomic DNA, the geometry of the clamp loader•DNA complex likely prevents the clamp loader from productively binding a closed clamp. In addition, binding of the bacterial and eukaryotic clamp loaders to p/t-DNA triggers rapid ATP hydrolysis and dissociation of the clamp loader from the DNA, such that the clamp loader•DNA complex is transient and not likely to be long-lived enough to efficiently bind clamps (75,97). Nonproductive interactions between the clamp loaders and DNA would reduce the overall efficiency of clamp loading by engaging the clamp loader in futile cycles of DNA binding and ATP hydrolysis. A mechanism that favored clamp binding prior to DNA binding would increase the overall efficiency of clamp loading. It is possible that the rate-limiting ATP-induced conformational changes that precede DNA binding but not clamp binding provide a kinetic preference for the clamp loader to bind the clamp before DNA and increase the overall efficiency of clamp loading.

The fastest rate at which the clamp loader can bind DNA is limited by rate of the ATP-induced conformational change (3.3 s^{-1}), but binding could be slower if DNA concentrations are limiting. The rate of the conformational change that promotes high affinity β binding is faster so that the rate of β binding may be a function of the concentration of β in the cell, 500 nM assuming 300 copies of β (98) in a 1 x 10^{-15} liter cell volume, and the bimolecular rate constant for binding, 2.3 x 10^{7} M^{-1} s^{-1}, to give an effective on-rate of 11 s^{-1}. This effective on-rate assumes that β on the lagging strand is rapidly recycled by excess δ subunit and/or clamp loader in the cell such that all the β is free to be loaded (59). Even at saturating concentrations of DNA, given these rates, γ complex would bind β first at least 75% of the time. During active replication, the timing of primer synthesis on the lagging strand could also provide a mechanism for regulating

the order of β and DNA binding. This could be accomplished by synthesizing primers at a rate that would allow the clamp loader to bind a clamp before a new primed template site is formed.

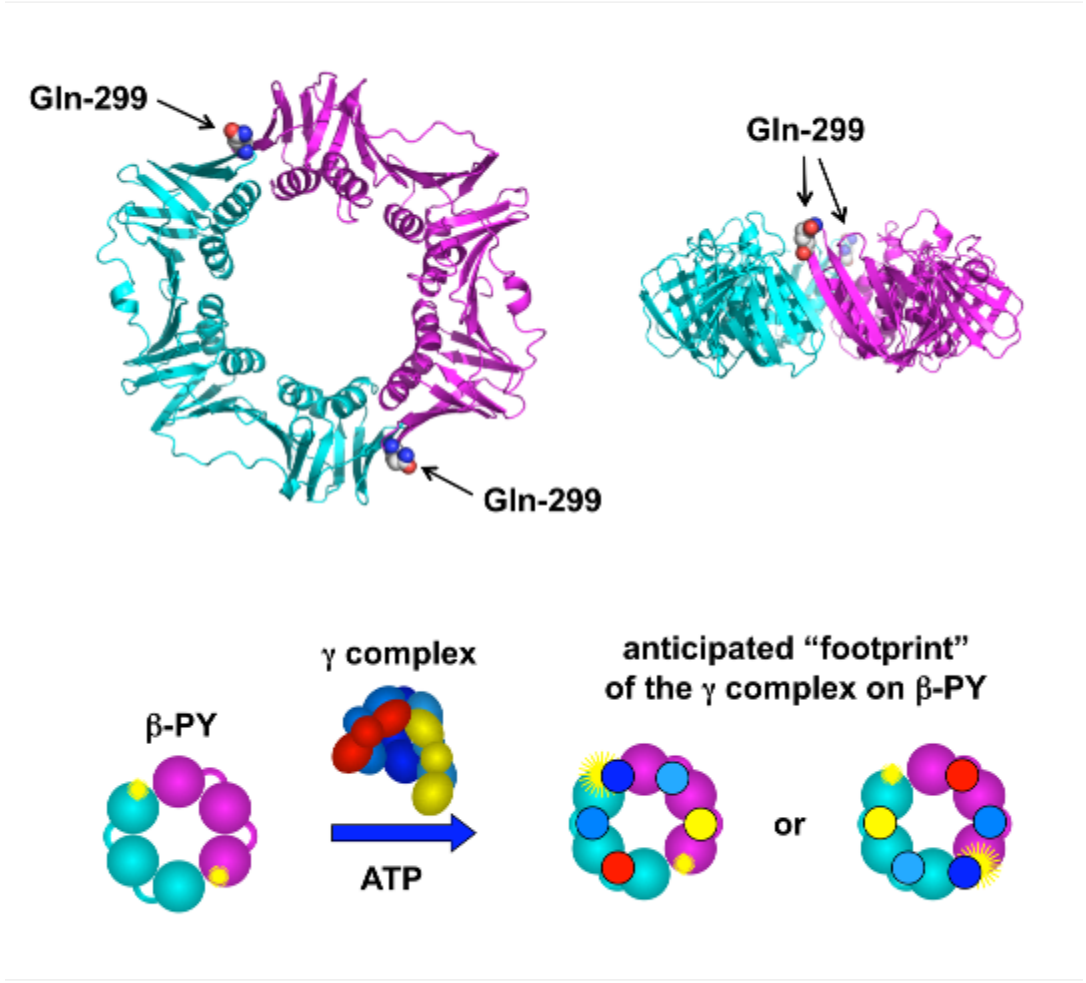

Figure 3-1. Fluorescence intensity-based β-clamp binding assay. *Upper panel*, A ribbon diagram of the β-clamp is shown with one monomer in cyan and the other in magenta. Glutamine-299 (spheres), located on the surface of β to which γ complex binds, was converted to cysteine. Two surface cysteines, Cys-260 and Cys-333 were converted to serine, so that Cys-299 could be selectively labeled with pyrene (PY). *Lower panel*, The β-clamp has a C2 axis of symmetry through the center of the ring such that two PY fluorophores (yellow starbursts) covalently attached to Cys-299 are located on opposite sides of the ring. When γ complex binds β-PY, one γ subunit (dark blue) likely binds at or near a PY to alter its environment and increase PY fluorescence (larger yellow starburst). The second PY molecule is unlikely to interact with γ complex so that only a single PY molecule is reporting on the binding interaction.

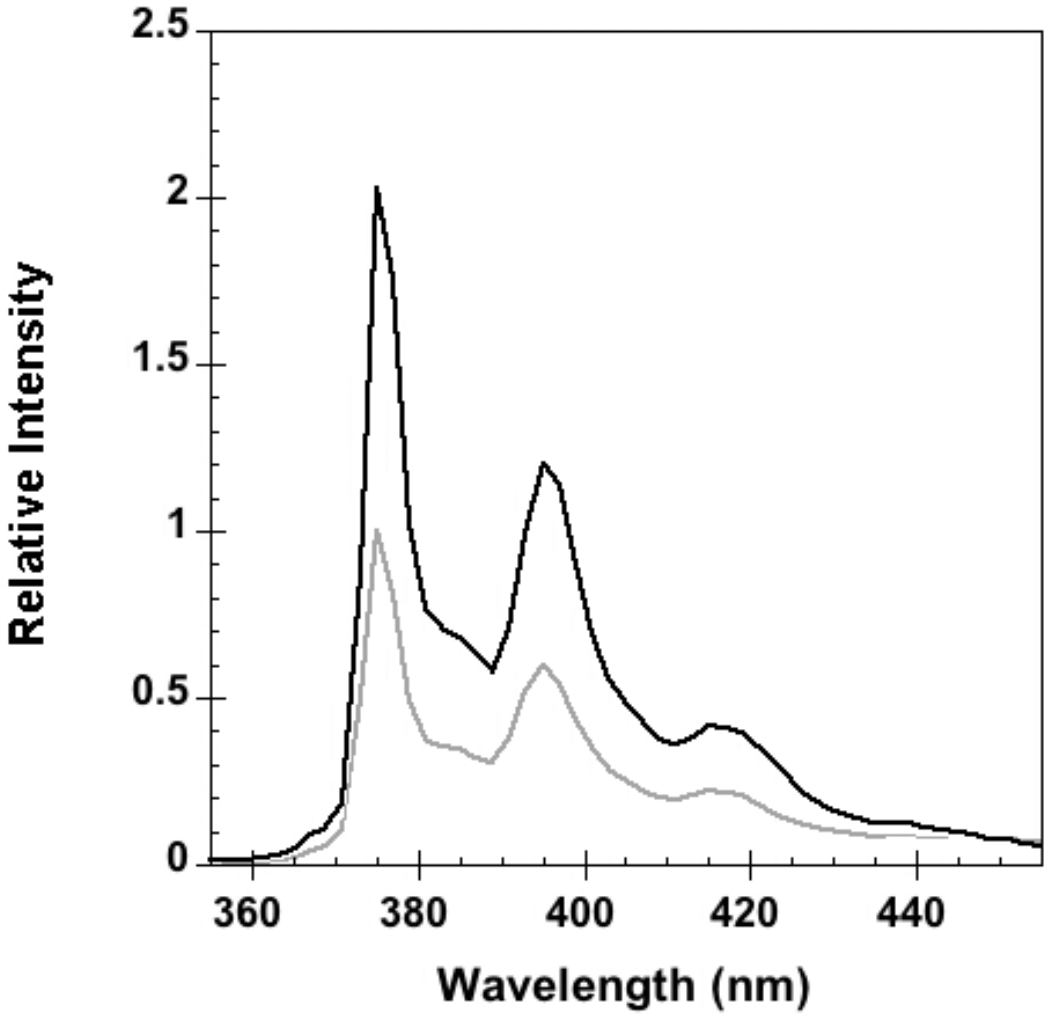

Figure 3-2. Emission Spectra of pyrene fluorescence. Emission spectra of β-PY were taken at excitation wavelength of 345 nm. The *light gray trace* is a scan of free β-PY and the *black trace* is after the addition of γ complex and ATP. Final concentrations were 80 nM β-PY, 240 nM γ complex, and 0.5 mM ATP.

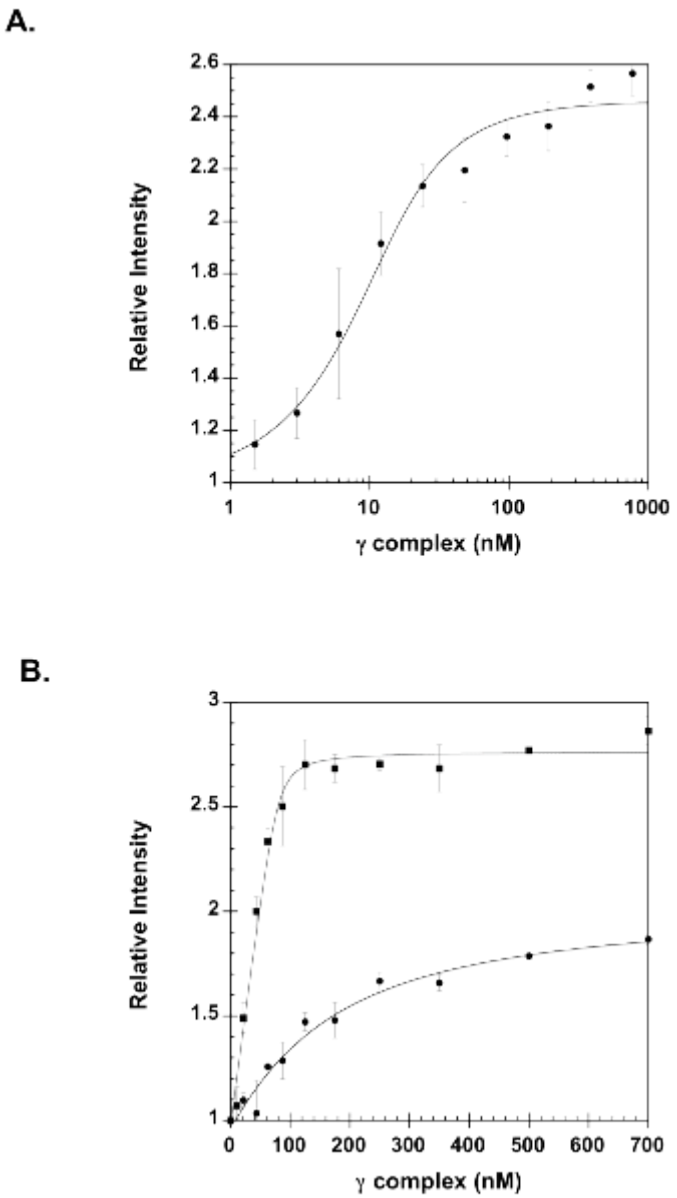

Figure 3-3. Equilibrium binding of γ complex to β. A) Equilibrium binding of γ complex to β was determined by measuring the intensity of PY as a function of γ complex concentration, where γ complex was titrated into β-PY in assay buffer containing ATP. Final concentrations were 10 nM β-PY and 0.5 mM ATP in assay buffer. B) Stoichiometric binding of γ complex to β was measured in the absence (circles) and presence (squares) of ATP. The γ complex and ATP were added sequentially to a solution of β-PY in assay buffer. The intensity of PY is plotted as a function of γ complex concentration. Final concentrations after the addition of ATP were 80 nM β-PY and 0.5 mM ATP in assay buffer.

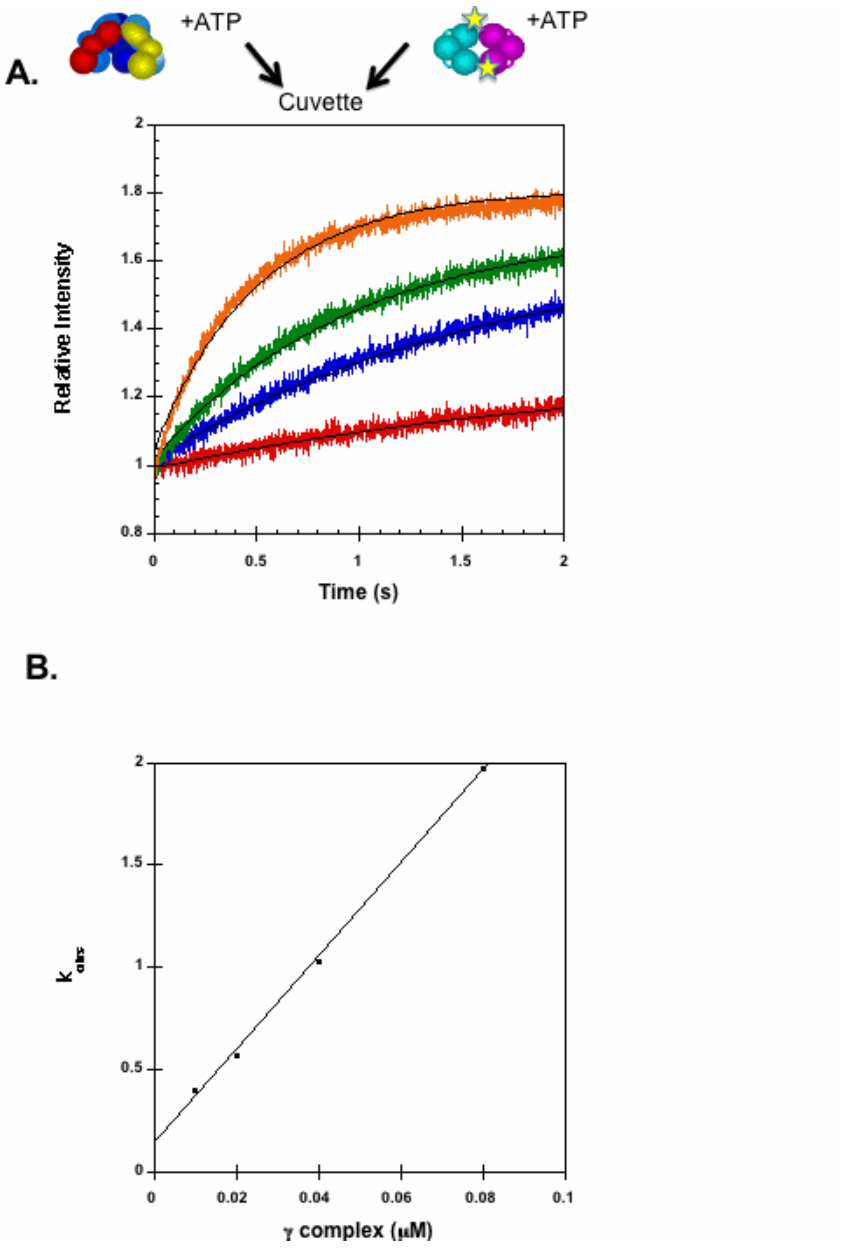

Figure 3-4. Kinetics of γ complex binding to β-PY. A) The increase in PY intensity was measured as a function of time when a solution of γ complex and ATP (0.5 mM) was added directly to a solution of β-PY and ATP (0.5 mM). Reactions contained 20 nM β-PY and 10 nM (red), 20 nM (blue), 40 nM (green), or 80 nM (orange) γ complex in assay buffer with 4% glycerol. Solid black lines through time courses are the result of an empirical fit of the data to an exponential rise. B) Observed rate constants, k_{obs}, calculated from exponential fits of the reaction time courses are plotted against the concentration of γ complex. A linear fit of these data gave a slope of 22.7 $\mu M^{-1} s^{-1}$ and a y-intercept of 0.14 s^{-1}.

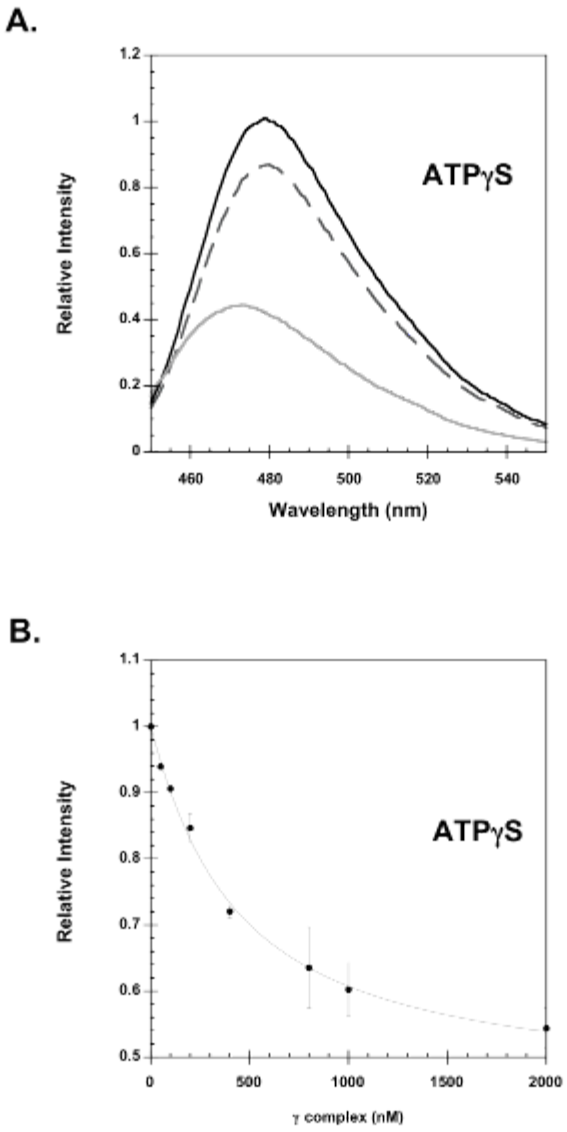

Figure 3-5. Binding of γ complex to DNA. A) Emission spectra of DCC were measured using an excitation wavelength of 455 nm. The *black trace* is a scan of free p/t-DNA-DCC, the *dashed dark gray trace* is a scan repeated after the addition of 200 nM γ complex, and the *light gray trace* is a scan repeated after the addition of ATPγS. Final concentrations were 100 nM p/t-DNA-DCC, 200 nM γ complex, and 0.5 mM ATPγS in assay buffer. B) The relative intensity of DCC in a clamp loader•DNA complex was determined by measuring DCC fluorescence as a function of γ complex concentration. The maximal quench in DCC fluorescence was calculated by fitting these data to a quadratic equation (*Materials and Methods*). The solid line through the data is the result of the fit, which gave a value of 0.58 for the relative intensity of DCC in a clamp loader•DNA complex and a K_D value of 375 ± 7 nM for clamp loader•DNA dissociation. Final concentrations were 100 nM p/t-DNA-DCC and 0.5 mM ATPγS in assay buffer.

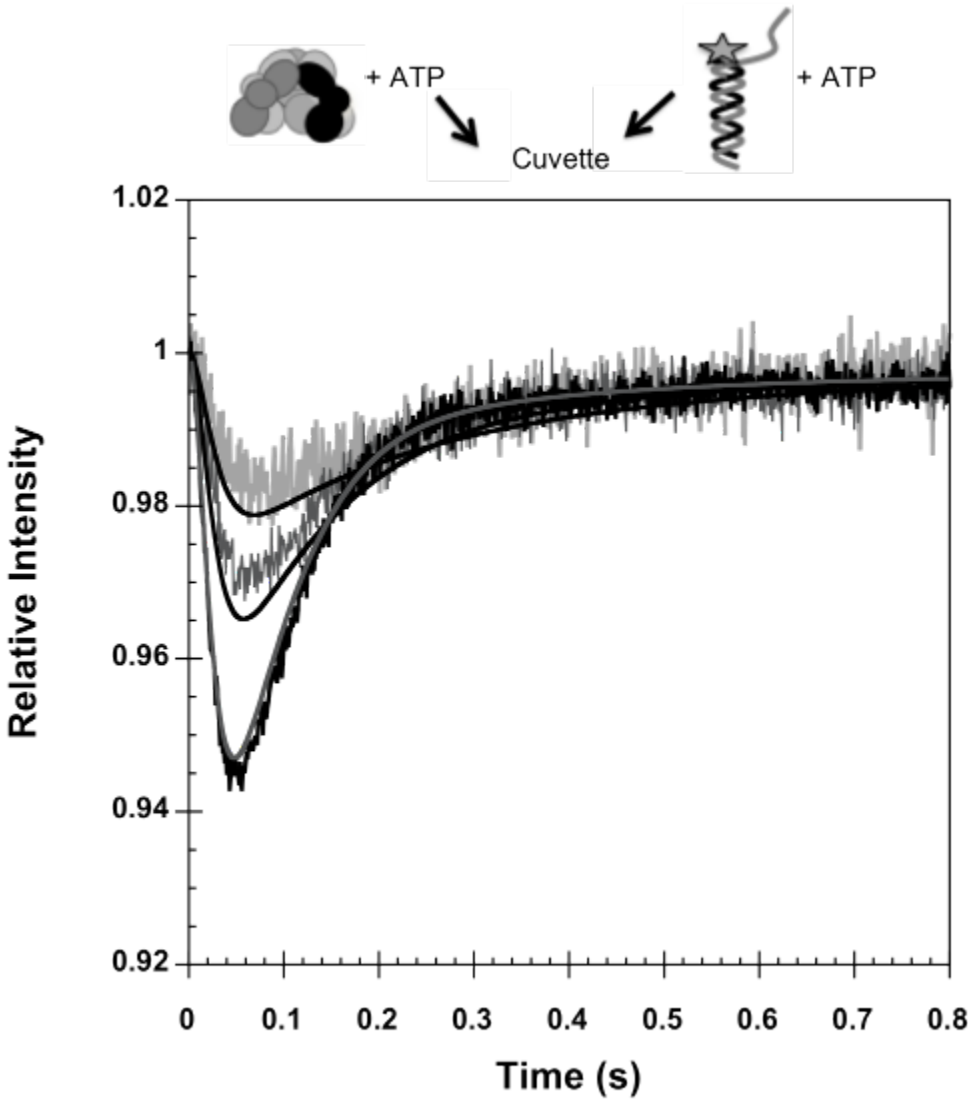

Figure 3-6. The rate of γ complex binding to DNA. The γ complex binding to DNA was measured in reactions in which a solution of γ complex and ATP was added to a solution of p/t-DNA-DCC and ATP. The relative fluorescence of DCC is plotted as a function of time. Final concentrations were 125, 250, 500 nM γ complex and p/t-DNA-DCC and 0.5 mM ATP in assay buffer with 4% glycerol. The concentrations of γ complex and DNA are indicated by the shade of gray; darker indicates a higher concentration. Solid lines through the reaction time course were generated from the kinetic model illustrated in Fig. 3-11.

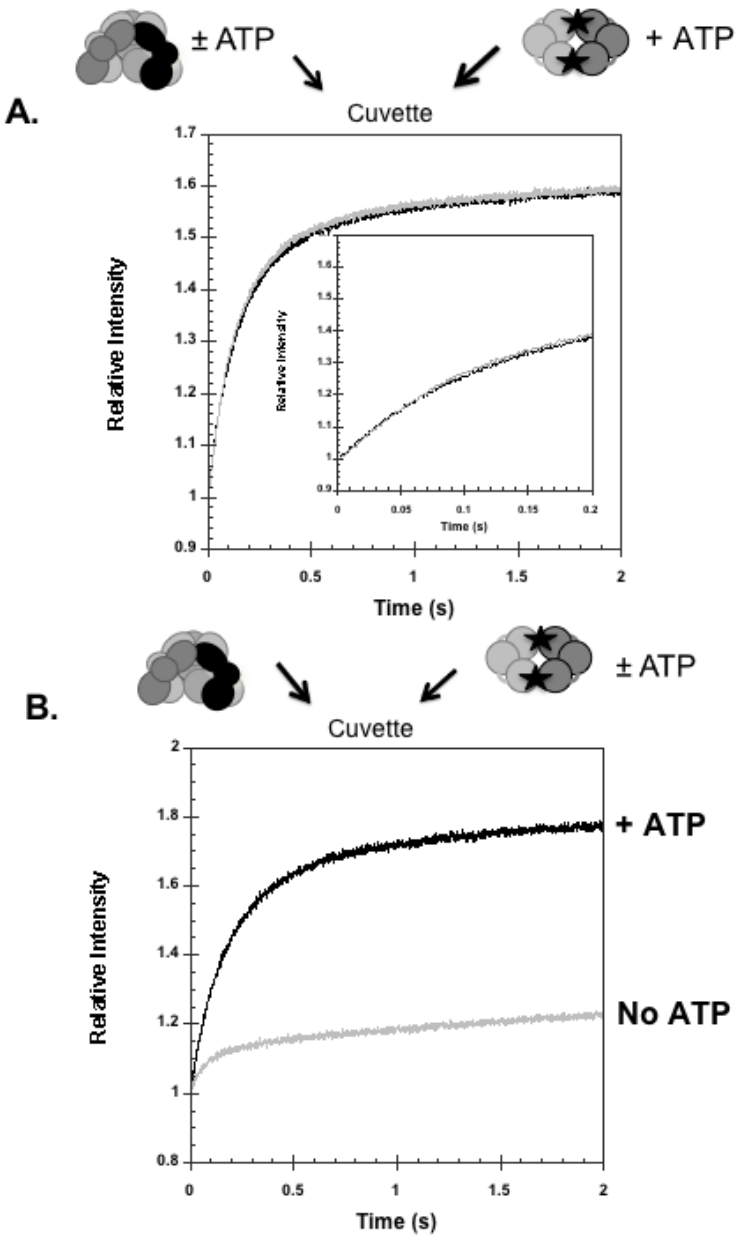

Figure 3-7. Rates of γ complex binding β with and without pre-incubation of γ complex with ATP. A) The rate of γ complex binding β-PY was measured in assays with (gray trace) and without (black trace) pre-incubation of γ complex and ATP. The relative intensity of PY is plotted as a function of time for a reaction in which a solution of γ complex and ATP was added to a solution of β-PY and ATP (gray trace) and a reaction in which a solution of γ complex was added to a solution of β-PY and ATP (black trace). The insert is the first 0.2 s of the reaction time courses. B) Rates of γ complex binding β-PY were measured in the absence of ATP (gray trace) and in the presence of ATP but without the pre-incubation of γ complex with ATP (black trace). Final concentrations were 200 nM β-PY and γ complex and 0.5 mM ATP in assay buffer with 4% glycerol.

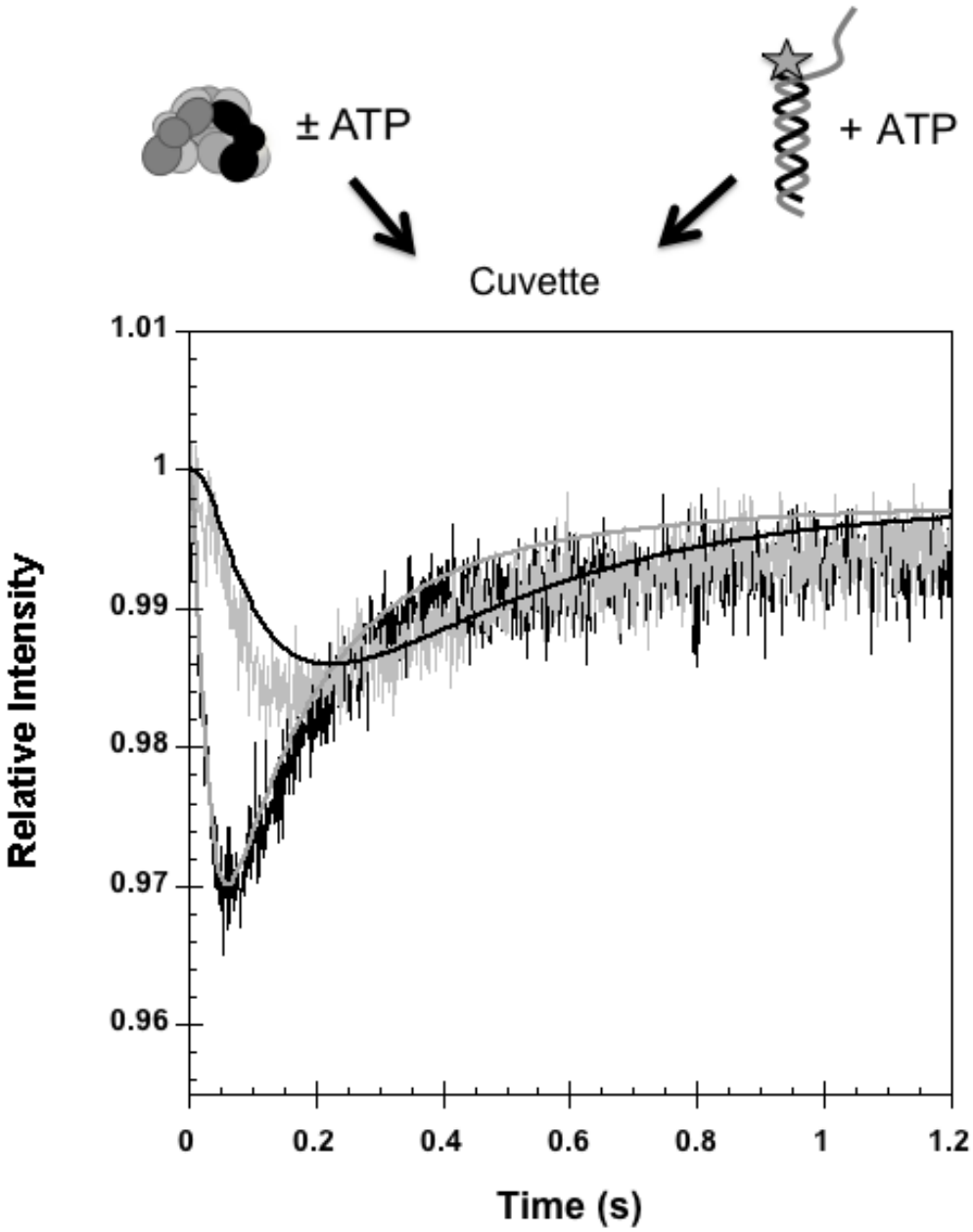

Figure 3-8. γ complex binding DNA with and without pre-incubation of γ complex with ATP. The change in DCC fluorescence due to γ complex binding DNA was measured as a function of time. In one assay (*black trace*), a solution of γ complex and ATP was added to a solution of p/t-DNA-DCC and ATP. In the second (*gray trace*), a solution of γ complex that did not contain ATP was added to a solution of p/t-DNA-DCC and ATP. The relative intensity of DCC is plotted as a function of time on a scale of 2 s. Final concentrations were 200 nM p/t-DNA-DCC and γ complex, and 0.5 mM ATP in assay buffer with 4% glycerol. Smooth solid lines through the data are from a fit to the model in Fig. 3-11.

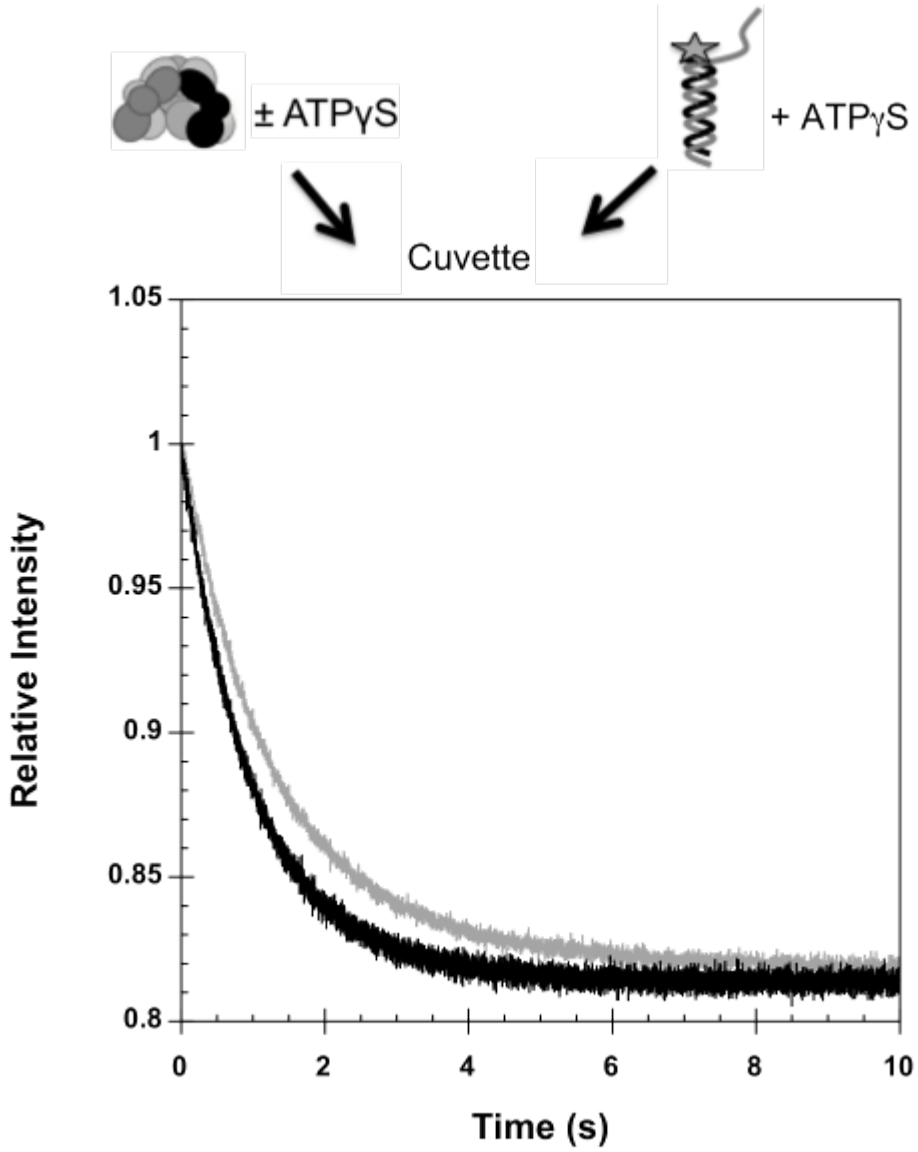

Figure 3-9. Effect of ATPγS preincubation on the rate of γ complex binding p/t-DNA-DCC. The change in DCC fluorescence due to γ complex binding DNA was measured as a function of time. In one assay (*black trace*), a solution of γ complex and ATPγS was added to a solution of p/t-DNA-DCC and ATPγS. In the second (*gray trace*), a solution of γ complex that did not contain ATPγS was added to a solution of p/t-DNA-DCC and ATPγS. The relative intensity of DCC is plotted as a function of time on a scale of 2 s. Final concentrations were 200 nM p/t-DNA-DCC and γ complex, and 0.5 mM ATPγS in assay buffer with 4% glycerol.

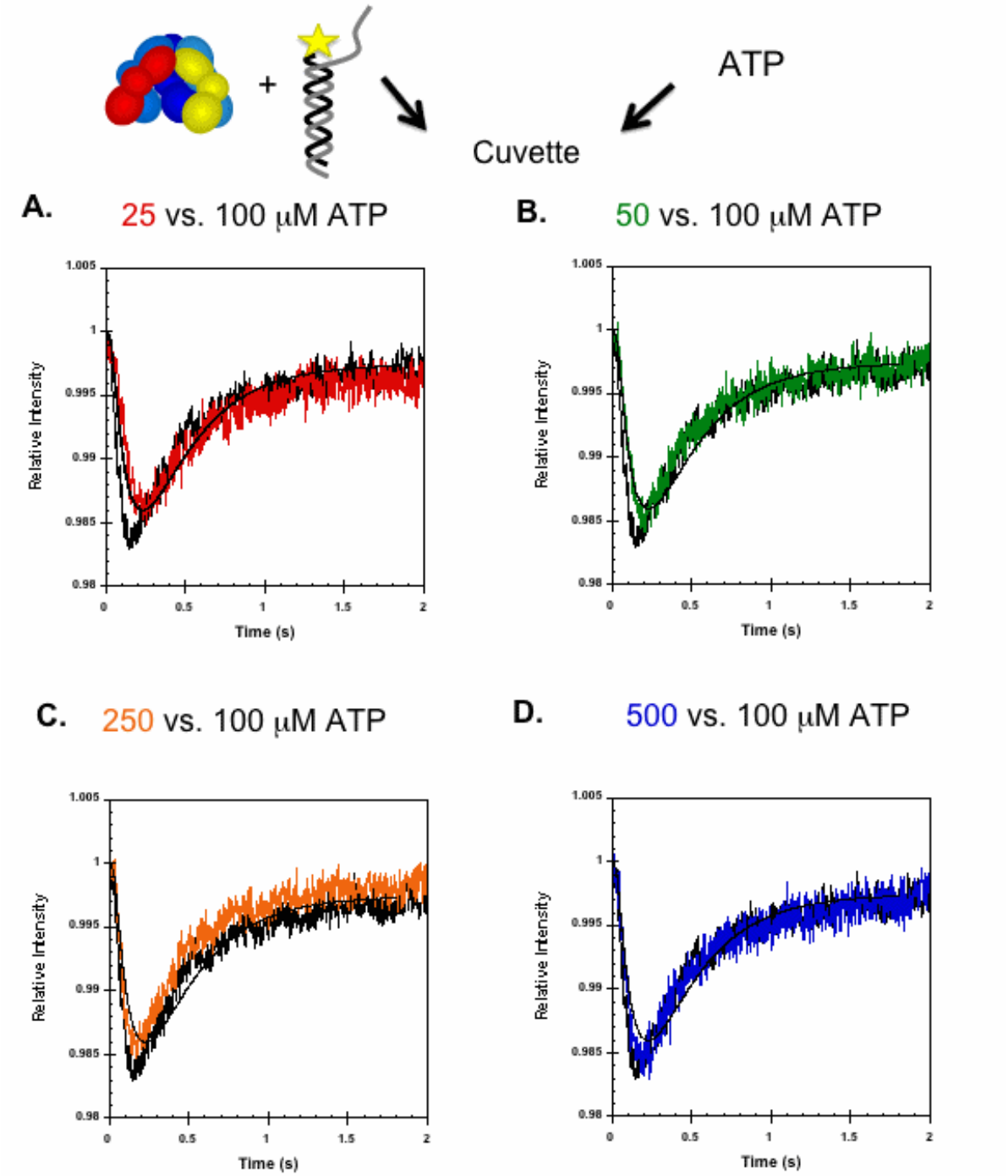

Figure 3-10. Effect of ATP concentration on γ complex•DNA binding kinetics. Rates of DNA binding were measured as a function of ATP concentration in a reaction in which γ complex was not pre-incubated with ATP. A solution of γ complex and p/t-DNA-DCC was mixed with a solution of ATP and the DCC fluorescence was measured as a function of time. Final concentrations were 200 nM p/t-DNA-DCC and γ complex, and A) 25 μM, B) 50 μM, C) 250 μM, and D) 500 μM ATP relative to the same reaction at 100 μM ATP (*black trace*) in assay buffer with 4% glycerol. Smooth black lines through the data are from a fit to the model in Fig. 3-11.

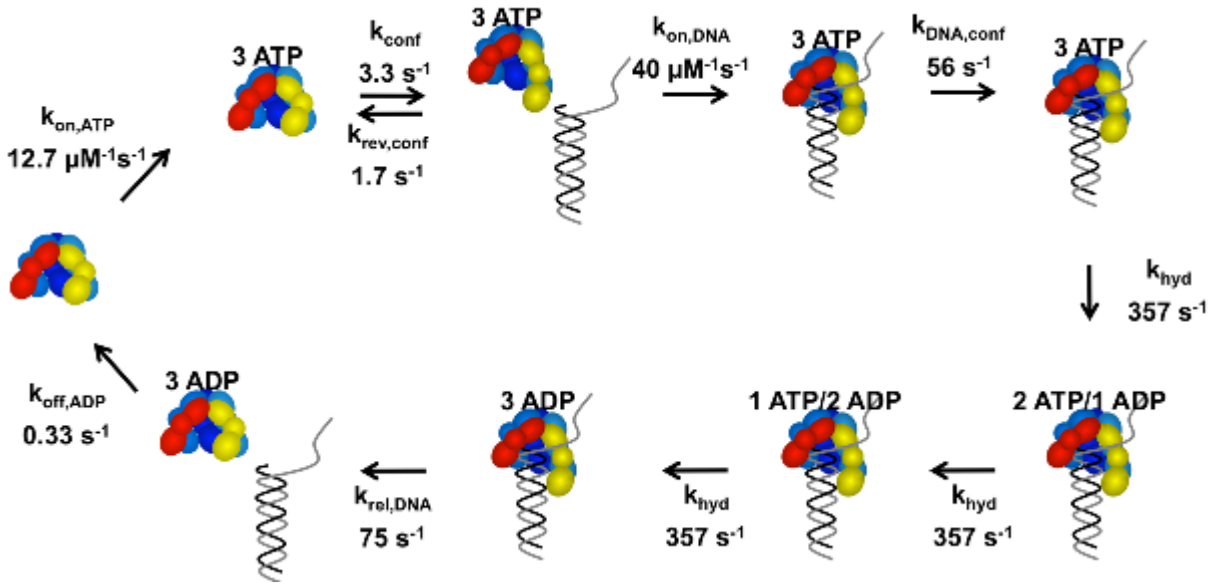

Figure 3-11. Kinetic model fit to p/t-DNA binding data. The model starts on the left-hand side with free γ complex. (Note: The γ complex used in our studies contains seven polypeptides, $\gamma_3\delta\delta'\chi\psi$, but only five, $\gamma_3\delta\delta'$, are illustrated in the diagram). The γ complex binds 3 molecules of ATP, as a unit at in a single step. ATP binding promotes a conformational change that allows the clamp loader to bind DNA. DNA binding induces a second conformational change that activates the ATP sites for hydrolysis and three molecules of ATP are hydrolyzed sequentially at the same rate. DNA and then ADP are released to allow γ complex to recycle. The relative intensity of free DNA was set at 1 and the relative intensities for all bound DNA species set at 0.58. The data in Figs. 3-6, 3-8, and 3-10 were fit to this model using DynaFit (89).

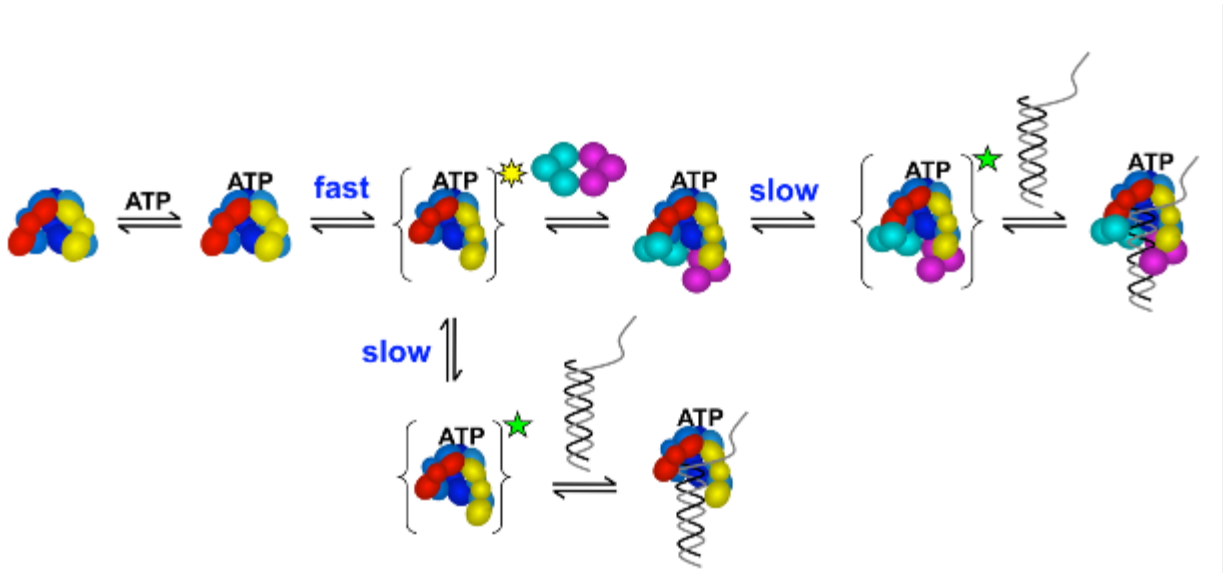

Figure 3-12. Model for formation of a ternary clamp loader•clamp•DNAcomplex**.** ATP binds the clamp loader and rapidly induces a conformational change (*yellow star state*) that enables the clamp loader to bind the clamp. A second conformational change (*green star state*) occurs more slowly and enables the clamp loader to bind p/t-DNA. This second conformational change could either occur within a clamp loader-clamp complex when the clamp is present (*upper reaction scheme*), or within the free clamp loader in the absence of the clamp (*lower reaction scheme*) to promote p/t-DNA binding. Note that the γ complex can bind three molecules of ATP, but that we have not determined how many molecules bind at each stage of the assembly reaction. Therefore, the stoichiometry of bound ATP molecules at each step is not given. It is possible that the slow conformational change opens an ATP site, or a subset of sites, to allow binding of additional ATP that promotes DNA binding.

CHAPTER 4
DISCUSSION AND FUTURE STUDIES

Given that a different set of conformational changes gives rise to β and DNA binding, it will be interesting to see which conformational changes promote clamp opening. The first “fast” conformational change could promote both clamp binding and clamp opening as illustrated in Fig. 3-12. Alternatively, the second slower conformational change could promote clamp opening and subsequent DNA binding. We have recently developed a fluorescence intensity-based assay to measure γ complex•β opening and closing. Using this assay, we could potentially define the rate of opening and compare it to the rate of β binding and DNA binding.

There are a number of interesting observations in the literature that can be used to speculate about a mechanism by which two distinct sets of conformational changes could occur sequentially to promote β and then DNA binding. The γ complex has three ATP sites and sequential filling of these sites could promote sequential sets of conformational changes. A subset of ATP sites could fill first to induce conformational changes rapidly that promote β binding. A slow conformational change could then allow the remaining sites to fill with ATP and promote DNA binding. Incubation of γ complex with ATP prior to adding β or DNA would give all the sites time to fill with ATP and allow the conformational changes to occur so that γ complex could bind either the clamp or DNA.

Studies with arginine finger mutants of the *E. coli* and yeast clamp loaders, which bind but do not “sense” or respond to bound ATP, show that ATP binding at different sites has differential effects on clamp and DNA binding (72,99). Similarly, studies of single Walker A mutants that reduce ATP binding to the yeast clamp loader showed that

mutations of individual sites had differential effects on DNA binding (100). Both Arg finger (99) and Walker A (100) mutations that affect ATP sensing/binding to the replication factor C (RFC) 2 and RFC3 subunits of the yeast clamp loader gave the greatest decreases in DNA binding activities. Interestingly, Arg finger mutations in the *E. coli* clamp loader that affect ATP sensing in the γ subunit that occupies the same position as RFC3 (darkest blue or middle γ subunit in Fig. 3-12), as well as the γ subunit adjacent to the " subunit, greatly reduced DNA binding.

In a crystal structure of the minimal *E. coli* clamp loader ($\gamma_3\delta\delta'$), the middle γ subunit does not contain a bound ATPγS molecule, whereas the other two γ subunits are bound to ATPγS (44). Biochemical characterization showed that this minimal clamp loader ($\gamma_3\delta\delta'$) had greatly reduced DNA binding activity compared with γ complex ($\gamma_3\delta\delta'\chi\psi$), which is consistent with the idea that ATP binding to the middle γ subunit is important for DNA binding (61). That is not to say that a single subunit binds DNA, but instead that ATP binding at one (or a subset of sites) is important for inducing conformational changes within the clamp loader that as a whole increase DNA binding activity. If a slow conformational change were to open this site and cause it to fill last, then this could provide a mechanism for sequential binding of the clamp and DNA.

The observation that the rate of p/t-DNA binding is limited by the rate of ATP-induced conformational changes is consistent with results from previous work measuring rates of p/t-DNA-triggered ATP hydrolysis by γ complex. As with the DNA binding kinetics, we found that rates of DNA-triggered ATP hydrolysis were faster when γ complex was preincubated with ATP than when there was no ATP preincubation, and that the slower rate was not due to slow ATP binding (84). Based on rates of ATP

hydrolysis as a function of preincubation time with ATP, a forward rate constant of 6.5 s^{-1} and reverse rate constant of 3.9 s^{-1} was calculated for the ATP-induced conformational changes. These values are in good agreement with the values of 3.3 and 1.7 s^{-1} for the forward and reverse rate constants calculated from kinetic modeling of the DNA binding reaction (see Fig. 3-11) given both the complexity of this reaction and that the two data sets were fit independently. Both sets of experiments predict that after equilibration with ATP a little over 60% of the clamp loaders (63% from ATPase experiments and 66% from DNA binding experiments) exist in the conformational state that has high affinity for p/t-DNA. Interaction with the β clamp increases the affinity of the clamp loader for DNA, and it is interesting to speculate that the β clamp may do this by stabilizing the conformational state with a high affinity for DNA and shifting the equilibrium to favor this species (73).

Studies with a minimal form of the clamp loader, $\gamma_3\delta\delta'$, missing the χ and ψ subunits support this idea. The minimal clamp loader is defective in ATP-dependent DNA binding activity. The β clamp can rescue the ATP-dependent DNA binding activity of the minimal clamp loader most likely by stabilizing or promoting the conformational state with high affinity for DNA (61). It is likely that the β clamp also increases the affinity of the clamp loader for DNA by directly interacting with the DNA duplex. The central cavity of the β ring is lined with positively charged amino acid residues (13) and these residues interact with the sugar-phosphate backbone of the duplex (101).

APPENDIX
DEVELOPMENT OF A NEW FLUORESCENCE-BASED ASSAY: MEASURING PCNA OPENING IN THE *SACCHAROMYCES CEREVISIAE* DNA REPLICATION SYSTEM

Introduction

In *S. cerevisiae*, clamp loading is a dynamic, multistep process that leads to the formation of a ternary complex and ultimately the assembly of PCNA onto DNA to allow for processive replication (102). RFC must first be primed with ATP and undergo a conformational change that increases its affinity for binding PCNA. After binding ATP, RFC binds to PCNA and DNA to form a ternary RFC-PCNA-DNA complex. Alternatively, a similar set of conformational changes may trigger both PCNA binding and opening or PCNA opening and DNA binding at the same time or sequentially. The binding of RFC to DNA triggers hydrolysis of ATP in one or more of the ATP sites. Hydrolysis of ATP most likely causes another conformational change in RFC, which prompts it to lose affinity for PCNA and DNA. PCNA closes around DNA and RFC dissociates from the complex.

The eukaryotic clamp loader for replication, RFC, consists of five subunits (A-E) that are found in a similar arrangement to that of the bacterial clamp loader. Three alternative RFC complexes also exist in which the RFC A subunit is replaced by another protein including Rad24 in *S. cerevisiae* (Rad17 in humans), Cft18, and Elg1. Rad24-RFC functions at the DNA damage checkpoint during S-phase (104,106). This clamp loader interacts with and loads onto DNA an alternative clamp called the 9-1-1 complex. The heterotrimeric clamp is composed of Rad9, Rad1, and Hus1 in humans and *S. pombe* (115,116) and Ddc1, Rad17, and Mec3, respectively in *S. cerevisiae* (117). The loading of the 9-1-1 complex by Rad24-RFC starts the DNA damage checkpoint activation and signals the recruitment of ATR to the site of damage (118). Rad24-RFC

can bind to PCNA and unload it from DNA but cannot productively load PCNA onto DNA (115,119).

The other two alternative subunits are not well understood (103-106). The Ctf18-RFC complex is required for sister chromatid cohesion. Two additional proteins, Ddc1 and Ctf8, bind to Ctf18 and are recruited to RFC to form a seven-subunit complex (105,107,108). Ctf18-RFC, both the five and seven-subunit complexes, can load and unload PCNA onto DNA (109-111). The Elg1-RFC alternative complex suppresses chromosomal rearrangements and plays a role in chromosome stability (112-114). A productive Elg1-RFC•PCNA interaction has not been demonstrated *in vitro* although protein interaction between Elg1 and PCNA was confirmed by co-immunoprecipitation (112). It is still unclear whether there is an alternative clamp that mainly interacts with this clamp loader or if PCNA is the main target for interaction.

Different RFC A subunits can be swapped out in an RFC complex to have different functions in the cell. Each new RFC complex has specificity for and interacts with PCNA or an alternative clamp in some way. In this work, the question of the contribution of the RFC A subunit in the RFC complex to the interaction with PCNA will be addressed by measuring clamp loader-clamp opening and closing.

A fluorescence-intensity based assay to measure opening and closing of an RFC•PCNA complex

A sensitive intensity-based fluorescence assay was developed to measure clamp loader•clamp opening and closing in the *S. cerevisiae* replication system. In this assay, residues Ile111 and Ile 181, located on opposite sides of the interfaces in PCNA (Fig. A-1), were mutated to Cys, and Cys-111 and Cys-181 were covalently labeled with Alexa Fluor 488, C_5 maleimide (AF488). These mutations were placed in a PCNA mutant with

three of the four naturally occurring Cys residues (Cys-22, Cys-62, and Cys-81) converted to Ser to allow for selective labeling. The PCNA mutant was labeled in the presence of a reducing agent tris (2-carboxyethyl) phosphine (TCEP), which does not react with maleimides, to prevent disulfide bond formation between the closely spaced cysteines. Two AF488 fluorophores are able to stack and self-quench when in physical contact. Based on available structural data for the yeast clamp, α-carbon atoms of residues 111 and 181 are located within 5.5 Å from each other.

Each PCNA monomer is labeled with two fluorophores per monomer. The homotrimer contains six fluorophores with a pair located at each monomer interface. Physical interaction of the fluorophores on either side of a monomer interface will quench AF488 fluorescence, and physical separation of these fluorophores should increase fluorescence. One mechanism to physically separate the fluorophores is by physical denaturation with a detergent. When a 5% SDS solution was added to PCNA-AF488, the fluorescence increased. The fluorescence of the denatured PCNA-AF488 in SDS was 8.6-fold greater than the fluorescence of AF488 in the native protein (Fig. A-2).

The clamp loader can physically separate fluorophores on either side of a monomer interface by opening the clamp. When RFC binds to PCNA-AF488 in the presence of ATP, AF488 fluorescence increases due to the formation of an open clamp loader-clamp complex (Fig. A-3, red). At saturating concentrations of RFC, the intensity of AF488 is about two-fold greater. A control experiment in which buffer was added in place of RFC gave a decrease in fluorescence due to dilution (Fig. A-3, blue). The fluorescence intensity of an open RFC•PCNA complex is less than the denatured

clamp, which is presumably due to only one of the three interfaces opening and showing a relief of quench. The increase in AF488 fluorescence was used to measure equilibrium binding of RFC to PCNA-AF488 and calculate the dissociation constant for the interaction. A K_D value of 13.0 ± 2.4 nM was calculated from three independent experiments at 10 nM PCNA-AF488 (average values are shown in Fig. A-4).

Measuring Rad24-RFC•PCNA Interactions using the PCNA-AF488 Opening Assay

Previous studies have shown that Rad24-RFC can unload PCNA from a circular DNA plasmid but cannot load PCNA onto DNA (119). Even though there was no loading detected, the Rad24-RFC ATPase was stimulated by PCNA (117); therefore, there is some interaction between Rad24-RFC and PCNA. The unloading of PCNA from a plasmid DNA was used as an indirect measurement of PCNA opening to determine whether Rad24-RFC binds and then opens the clamp. One disadvantage of using an indirect method to measure opening, is that stable open complexes of Rad24-RFC•PCNA maybe not be forming. Simply, PCNA may be transiently opening and closing and can easily slip off of the DNA or that Rad24-RFC transiently opens PCNA. The newly developed PCNA-AF488 opening assay would be useful to measure directly if Rad24-RFC opens PCNA to form a stable open complex.

A preliminary opening assay experiment was performed and the AF488 fluorescence was used to measure equilibrium binding of wild type RFC or Rad24-RFC to PCNA-AF488. The calculated dissociation constants for the interactions were then compared between the two RFC complexes. A K_D value of 76 nM was calculated for Rad24-RFC•PCNA while a K_D value of 13 nM was calculated for wild type RFC at 10 nM PCNA-AF488. The Rad24-RFC complex has about a six-fold weaker interaction with PCNA than wild type RFC. Based on the relative fluorescence intensity differences,

Rad24-RFC has a reduced ability to open PCNA compared to RFC. We currently cannot determine the absolute percentage of stable open clamp complexes in either the wild type RFC or Rad24-RFC cases, but the data suggests that there is about five times more open PCNA in a complex with RFC than in a complex with Rad24-RFC. This will be investigated further and will be interesting to see if we can further quantify the reduced amount of opening by Rad24-RFC compared to wild type RFC.

Discussion and Future Studies

The PCNA-AF488 opening assay will be useful for studying the initial and final steps of the clamp loading reaction: 1) binding and opening and 2) closing and release in steady state and pre-steady state experiments. Although basic characterization of this new mutant PCNA has been done, additional experiments are required to determine if PCNA-AF488 has wild type PCNA activity. One such experiment would be a competition binding assay in which the labeled clamp competes with the unlabeled clamp to bind RFC.

Many proteins that bind clamps interact through a conserved peptide sequence motif. Based on sequence alignments and binding studies, this motif is proposed to be Qxx (I/L/M) xxF (F/Y) for PCNA, termed the PCNA Interacting Peptide box (PIP box) (29-31). An important feature of this binding motif is the presence of hydrophobic amino acid residues including phenylalanine and tyrosine, which come in contact with the hydrophobic pocket on the clamp under an IDCL (32-34). Through sequence alignment studies, the RFC1 (A) subunit in yeast has a proposed PIP motif of NMSVVGYF. Using an additional method to test the importance of the RFC A subunit in the opening of PCNA, the two aromatic residues (tyrosine and phenylalanine) of the RFC1 (A) PIP motif will be mutated to alanine residues to disrupt the binding interaction with PCNA. If

the RFC A subunit is essential for opening PCNA, this RFC1 (A) PIP mutant will have a reduced opening ability, which will be tested using the PCNA-AF488 opening assay. We anticipate that the mutant will have a reduced ability to open PCNA as we have observed for Rad24-RFC, which has the RFC A subunit replaced with Rad24.

In addition to the PCNA-AF488 opening and closing assay, it will be useful to develop a PCNA binding assay as a method to compare the different steps in the clamp loading mechanism. Based on the available yeast RFC•PCNA crystal structure, a proposed site of mutation would be serine 43 on PCNA, which is at a site of interaction with RFC1. The Ser 43 residue would be mutated using site-direct mutagenesis to a cysteine into a PCNA with three of the four naturally occurring Cys residues (Cys-22, Cys-62, and Cys-81) converted to Ser to allow for selective labeling. The Ser 43 Cys residue would be labeled with an environmentally sensitive fluorophore that would potentially change in fluorescence upon binding to RFC. It will be interesting to use both the binding and opening assays in steady state and pre-steady state conditions to define the role of the RFC A subunit in the clamp loading reaction.

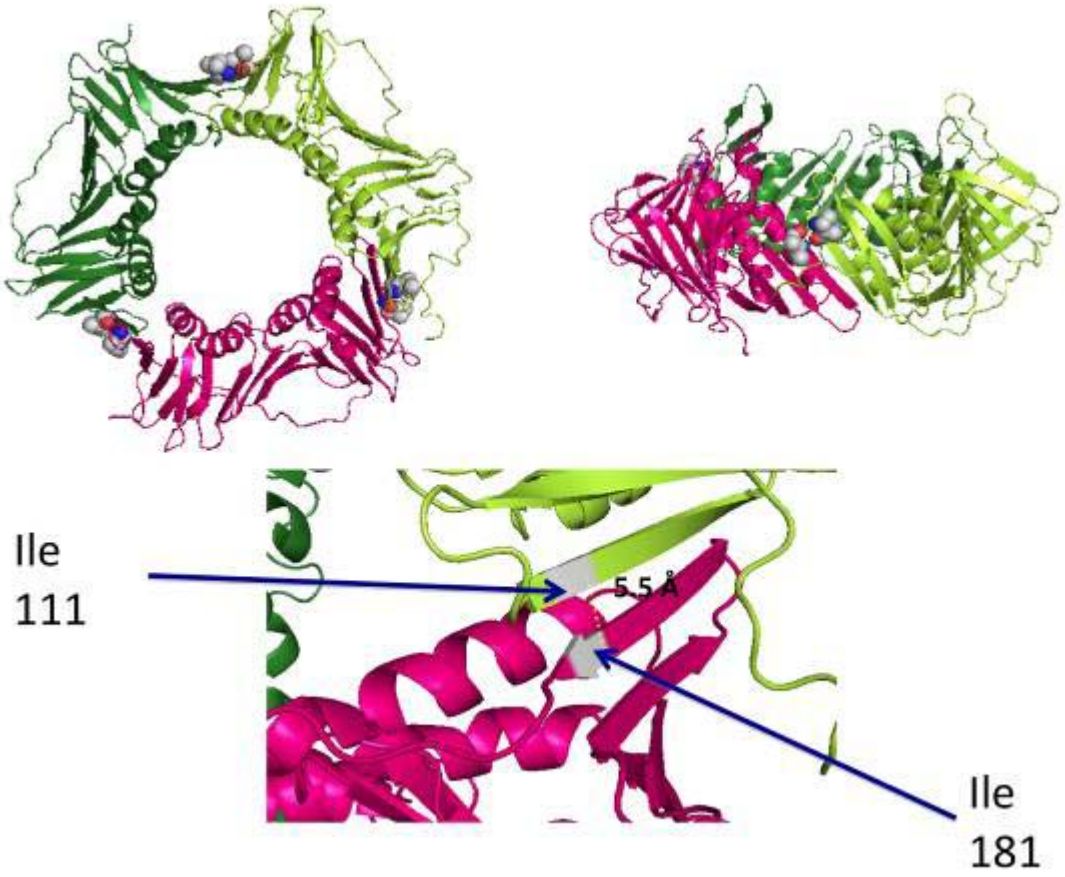

Figure A-1. Crystal Structural Model of PCNA highlighting the residues mutated for the PCNA opening assay. Residues Ile-111 and Ile-181 are located on opposite sides of the PCNA monomer interfaces. The distance between α-carbon atoms is about 5.5 Å. These residues were mutated to cysteines. Three of the naturally occurring Cys residues in PCNA were mutated to Ser to allow for selective labeling of these two residues. This creates two labeled residues per monomer, and a pair of fluorophores on each trimer interface. Structures were generated using PDB file 1SXJ (33).

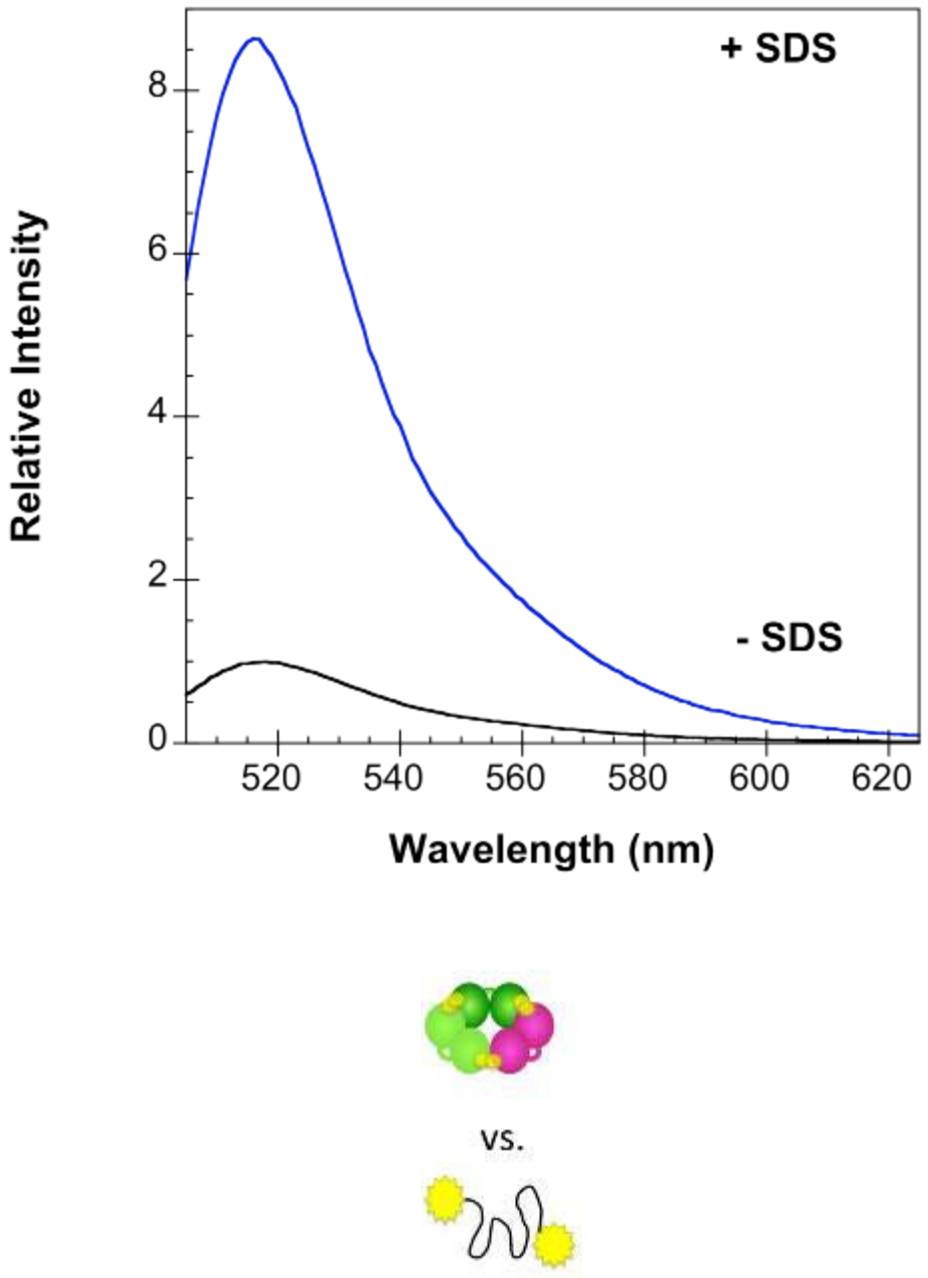

Figure A-2. Relief of the AF488 Fluorescence quench in the presence of SDS. Denaturation of PCNA-AF488 in 5% SDS solution increases the fluorescence of AF488 in the doubly-labeled clamp by about 8.6-fold. Solutions contained 10 nM PCNA-AF488 ± 5% SDS.

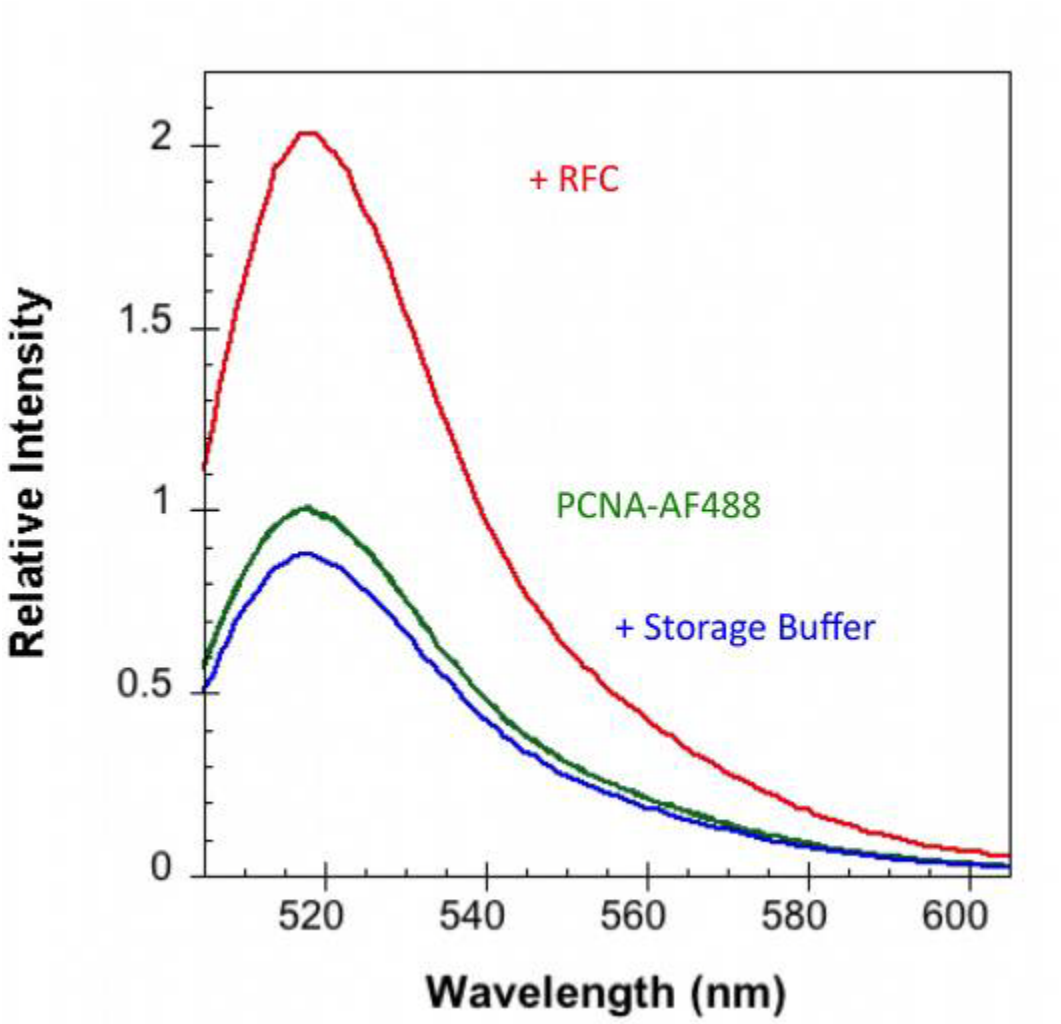

Figure A-3. Emission spectra of PCNA-AF488 were taken at excitation wavelength of 495 nm. The *green trace* is a scan of free PCNA-AF488, the *red trace* is after the addition of RFC and ATP, and the *blue trace* is after the addition of storage buffer and ATP instead of RFC. Final concentrations were 10 nM PCNA-AF488, 285 nM RFC, and 0.5 mM ATP.

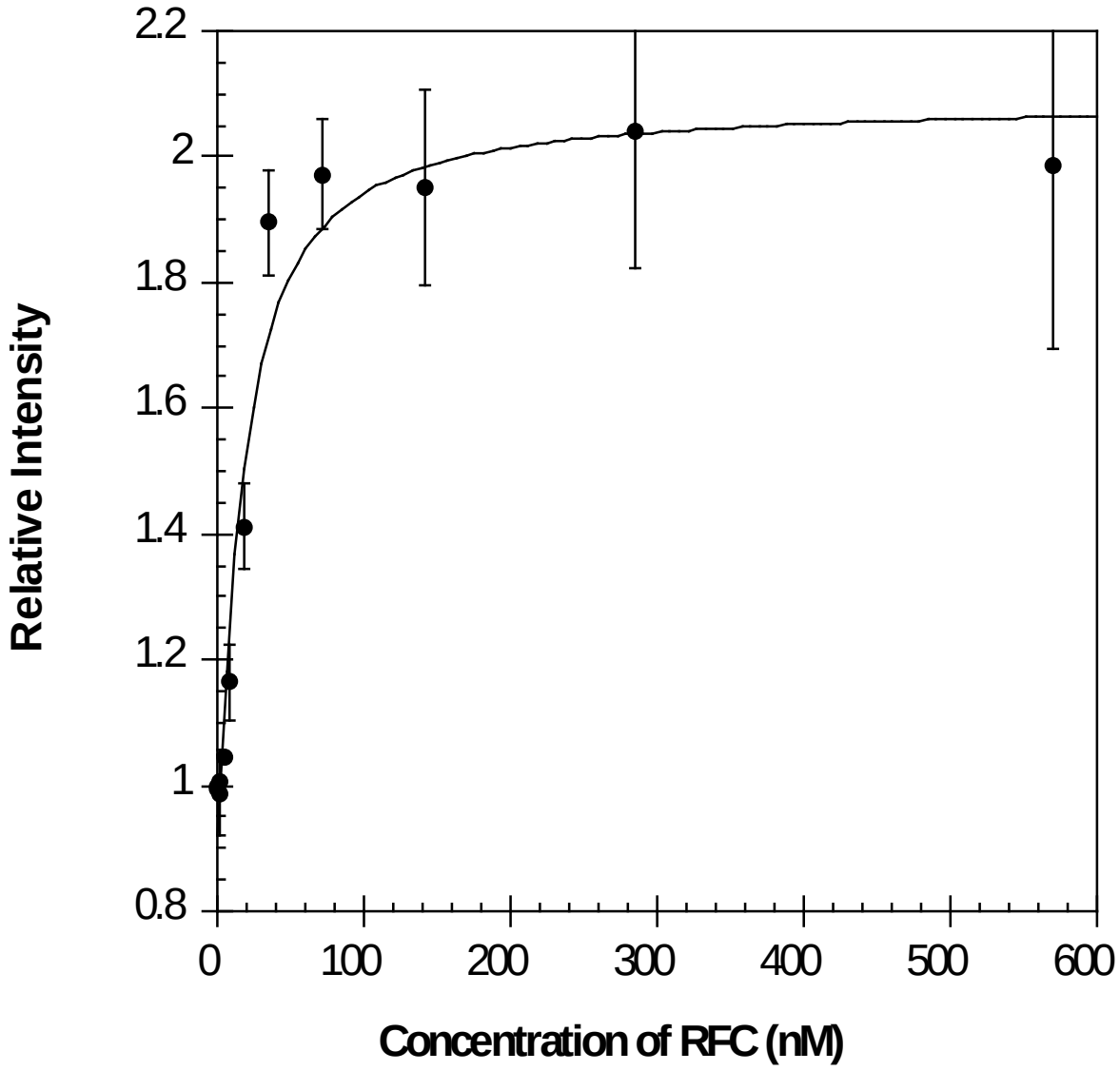

Figure A-4. Equilibrium binding and opening of RFC•PCNA. The equilibrium dissociation constant was determined by measuring the intensity of AF488 as a function of RFC concentration, where RFC was titrated into PCNA-AF488 in assay buffer containing ATP. Final concentrations were 10 nM PCNA-AF488 and 0.5 mM ATP in assay buffer.

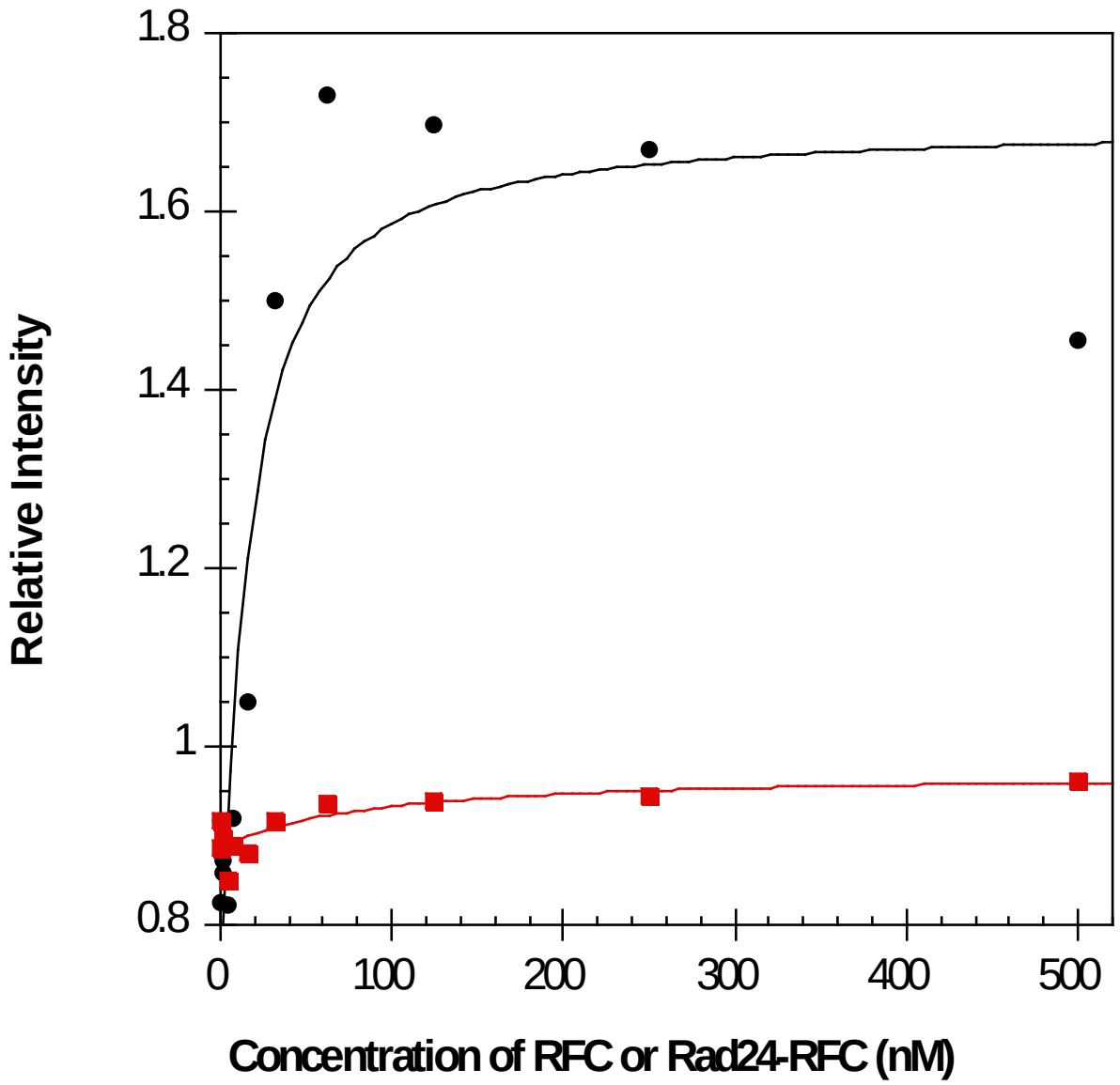

Figure A-5. Equilibrium binding and opening of Rad24-RFC•PCNA. The equilibrium dissociation constant for Rad24-RFC•PCNA (*red squares*) was compared with wild type RFC•PCNA (*black circles*) and was determined by measuring the intensity of AF488 as a function of Rad24-RFC or RFC concentration, where Rad24-RFC or RFC was titrated into PCNA-AF488 in assay buffer containing ATP. Final concentrations were 10 nM PCNA-AF488 and 0.5 mM ATP in assay buffer.

REFERENCE LIST

1. Kornberg, A. (1988) *J. Biol. Chem.* **263**, 1-4
2. Pomerantz, R. T., and O'Donnell, M. (2007) *Trends Microbiol* **15**, 156-164
3. Rowen, L., and Kornberg, A. (1978) *J. Biol. Chem.* **253**, 758-764
4. Arai, K., and Kornberg, A. (1979) *Proc. Natl. Acad. Sci. (USA)* **76**, 4308-4312
5. Lohman, T. M., and Bjornson, K. P. (1996) *Annu Rev Biochem* **65**, 169-214
6. Matson, S. W., and Kaiser-Rogers, K. A. (1990) *Annu Rev Biochem* **59**, 289-329
7. Patel, S. S., and Picha, K. M. (2000) *Annu Rev Biochem* **69**, 651-697
8. Chang, P., and Marians, K. J. (2000) *J. Biol. Chem.* **275**, 26187-26195
9. McHenry, C. S. (1982) *J. Biol. Chem.* **257**, 2657-2663
10. Johnson, A., and O'Donnell, M. (2005) *Annu Rev Biochem* **74**, 283-315
11. McHenry, C. S. (2003) *Mol Microbiol* **49**, 1157-1165
12. Hurwitz, J., and Wickner, S. (1974) *Proc. Natl. Acad. Sci. (USA)* **71**, 6-10
13. Kong, X.-P., Onrust, R., O'Donnell, M., and Kuriyan, J. (1992) *Cell* **69**, 425-437
14. Studwell-Vaughan, P. S., and O'Donnell, M. (1991) *J. Biol. Chem.* **266**, 19833-19841
15. Labib, K., and Gambus, A. (2007) *Trends Cell Biol* **17**, 271-278
16. Diffley, J. F. (2004) *Curr Biol* **14**, R778-786
17. Bochman, M. L., and Schwacha, A. (2009) *Microbiol Mol Biol Rev* **73**, 652-683
18. Aparicio, T., Ibarra, A., and Mendez, J. (2006) *Cell Div* **1**, 18
19. Pursell, Z. F., Isoz, I., Lundstrom, E. B., Johansson, E., and Kunkel, T. A. (2007) *Science (New York, N.Y* **317**, 127-130
20. Burgers, P. M. (2009) *J. Biol. Chem.* **284**, 4041-4045
21. Pavlov, Y. I., Frahm, C., Nick McElhinny, S. A., Niimi, A., Suzuki, M., and Kunkel, T. A. (2006) *Curr Biol* **16**, 202-207
22. Garg, P., Stith, C. M., Sabouri, N., Johansson, E., and Burgers, P. M. (2004) *Genes Dev* **18**, 2764-2773

23. Budd, M. E., and Campbell, J. L. (1997) *Mol. Cell Biol.* **17**, 2136-2142

24. Indiani, C., and O'Donnell, M. (2006) *Nat. Rev. Mol. Cell. Biol.* **7**, 751-761

25. Krishna, T. S., Kong, X.-P., Gary, S., Burgers, P. M., and Kuriyan, J. (1994) *Cell* **79**, 1233-1243

26. Shamoo, Y., and Steitz, T. A. (1999) *Cell* **99**, 155-166

27. Naktinis, V., Onrust, R., Fang, F., and O'Donnell, M. (1995) *J. Biol. Chem.* **270**, 13358-13365

28. Naktinis, V., Turner, J., and O'Donnell, M. (1996) *Cell* **84**, 137-145

29. Dalrymple, B. P., Kongsuwan, K., Wijffels, G., Dixon, N. E., and Jennings, P. A. (2001) *Proc. Natl. Acad. Sci. (USA)* **98**, 11627-11632

30. Warbrick, E. (1998) *BioEssays* **20**, 195-199

31. Warbrick, E. (2000) *BioEssays* **22**, 997-1006

32. Gulbis, J. M., Kelman, Z., Hurwitz, J., O'Donnell, M., and Kuriyan, J. (1996) *Cell* **87**, 297-306

33. Bowman, G. D., O'Donnell, M., and Kuriyan, J. (2004) *Nature* **429**, 724-730

34. Jeruzalmi, D., Yurieva, O., Zhao, Y., Young, M., Stewart, J., Hingorani, M., O'Donnell, M., and Kuriyan, J. (2001) *Cell* **106**, 417-428

35. Moldovan, G. L., Pfander, B., and Jentsch, S. (2007) *Cell* **129**, 665-679

36. Indiani, C., McInerney, P., Georgescu, R., Goodman, M. F., and O'Donnell, M. (2005) *Mol. Cell* **19**, 805-815

37. Lopez De Saro, F. J., Georgescu, R. E., Goodman, M. F., and O'Donnell, M. (2003) *EMBO J.* **22**, 6408-6418

38. Neuwald, A. F., Aravind, L., Spouge, J. L., and Koonin, E. V. (1999) *Genome Res* **9**, 27-43

39. Ogura, T., and Wilkinson, A. J. (2001) *Genes Cells* **6**, 575-597

40. Iyer, L. M., Leipe, D. D., Koonin, E. V., and Aravind, L. (2004) *J Struct Biol* **146**, 11-31

41. Hanson, P. I., and Whiteheart, S. W. (2005) *Nat. Rev. Mol. Cell. Biol.* **6**, 519-529

42. Erzberger, J. P., and Berger, J. M. (2006) *Annu Rev Biophys Biomol Struct* **35**, 93-114

43. Podobnik, M., Weitze, T. F., O'Donnell, M., and Kuriyan, J. (2003) *Structure (Camb)* **11**, 253-263

44. Kazmirski, S. L., Podobnik, M., Weitze, T. F., O'Donnell, M., and Kuriyan, J. (2004) *Proc. Natl. Acad. Sci. (USA)* **101**, 16750-16755

45. Jeruzalmi, D., O'Donnell, M., and Kuriyan, J. (2001) *Cell* **106**, 429-441

46. Kazmirski, S. L., Zhao, Y., Bowman, G. D., O'Donnell, M., and Kuriyan, J. (2005) *Proc. Natl. Acad. Sci. (USA)* **102**, 13801-13806

47. Miyata, T., Suzuki, H., Oyama, T., Mayanagi, K., Ishino, Y., and Morikawa, K. (2005) *Proc. Natl. Acad. Sci. (USA)* **102**, 13795-13800

48. Onrust, R., Finkelstein, J., Naktinis, V., Turner, J., Fang, L., and O'Donnell, M. (1995) *J. Biol. Chem.* **270**, 13348-13357

49. Pritchard, A. E., Dallman, H. G., Glover, B. P., and McHenry, C. S. (2000) *EMBO J.* **19**, 6536-6545

50. Blinkowa, A. L., and Walker, J. R. (1990) *Nucleic Acids Res.* **18**, 1725-1729

51. Flower, A. M., and McHenry, C. S. (1990) *Proc. Natl. Acad. Sci. (USA)* **87**, 3713-3717

52. Tsuchihashi, Z., and Kornberg, A. (1990) *Proc. Natl. Acad. Sci. (USA)* **87**, 2516-2520

53. O'Donnell, M. (2006) *J. Biol. Chem.* **281**, 10653-10656

54. Xiao, H., Dong, Z., and O'Donnell, M. (1993) *J. Biol. Chem.* **268**, 11779-11784

55. Olson, M. W., Dallmann, H. G., and McHenry, C. S. (1995) *J. Biol. Chem.* **270**, 29570-29577

56. Onrust, R., and O'Donnell, M. (1993) *J. Biol. Chem.* **268**, 11766-11772

57. Onrust, R., Stukenberg, P. T., and O'Donnell, M. (1991) *J. Biol. Chem.* **266**, 21681-21686

58. Tsuchihashi, Z., and Kornberg, A. (1989) *J. Biol. Chem.* **264**, 17790-17795

59. Leu, F. P., Hingorani, M. M., Turner, J., and O'Donnell, M. (2000) *J. Biol. Chem.* **275**, 34609-34618

60. Turner, J., Hingorani, M. M., Kelman, Z., and O'Donnell, M. (1999) *EMBO J.* **18**, 771-783

61. Anderson, S. G., Williams, C. R., O'Donnell, M., and Bloom, L. B. (2007) *J. Biol. Chem.* **282**, 7035-7045

62. Kelman, Z., Yuzhakov, A., Andjelkovic, J., and O'Donnell, M. (1998) *EMBO J.* **17**, 2436-2449

63. Yoder, B. L., and Burgers, P. M. (1991) *J. Biol. Chem.* **266**, 22689-22697

64. Fien, K., and Stillman, B. (1992) *Mol. Cell Biol.* **12**, 155-163

65. Cullmann, G., Fien, K., Kobayashi, R., and Stillman, B. (1995) *Mol. Cell Biol.* **15**, 4661-4671

66. Gomes, X. V., Gary, S. L., and Burgers, P. M. (2000) *J. Biol. Chem.* **275**, 14541-14549

67. Podust, V. N., Tiwari, N., Stephan, S., and Fanning, E. (1998) *J. Biol. Chem.* **273**, 31992-31999

68. Uhlmann, F., Cai, J., Gibbs, E., O'Donnell, M., and Hurwitz, J. (1997) *J. Biol. Chem.* **272**, 10058-10064

69. Fotedar, R., Mossi, R., Fitzgerald, P., Rousselle, T., Maga, G., Brickner, H., Messier, H., Kasibhatla, S., Hubscher, U., and Fotedar, A. (1996) *EMBO J.* **15**, 4423-4433

70. Podust, V. N., Tiwari, N., Ott, R., and Fanning, E. (1998) *J. Biol. Chem.* **273**, 12935-12942

71. Johnson, A., and O'Donnell, M. (2003) *J. Biol. Chem.* **278**, 14406-14413

72. Snyder, A. K., Williams, C. R., Johnson, A., O'Donnell, M., and Bloom, L. B. (2004) *J. Biol. Chem.* **279**, 4386-4393

73. Bloom, L. B., Turner, J., Kelman, Z., Beechem, J. M., O'Donnell, M., and Goodman, M. F. (1996) *J. Biol. Chem.* **271**, 30699-30708

74. Hingorani, M. M., and O'Donnell, M. (1998) *J. Biol. Chem.* **273**, 24550-24563

75. Ason, B., Bertram, J. G., Hingorani, M. M., Beechem, J. M., O'Donnell, M., Goodman, M. F., and Bloom, L. B. (2000) *J. Biol. Chem.* **275**, 3006-3015

76. Ason, B., Handayani, R., Williams, C. R., Bertram, J. G., Hingorani, M. M., O'Donnell, M., Goodman, M. F., and Bloom, L. B. (2003) *J. Biol. Chem.* **278**, 10033-10040

77. Maki, S., and Kornberg, A. (1988) *J. Biol. Chem.* **263**, 6547-6554

78. Dong, Z., Onrust, R., Skangalis, M., and O'Donnell, M. (1993) *J. Biol. Chem.* **268**, 11758-11765

79. Anderson, S. G., Thompson, J. A., Paschall, C. O., O'Donnell, M., and Bloom, L. B. (2009) *Biochemistry* **48**, 8516-8527

80. Johanson, K. O., Haynes, T. E., and McHenry, C. S. (1986) *J. Biol. Chem.* **261**, 11460-11465

81. Thompson, J. A., Paschall, C. O., O'Donnell, M., and Bloom, L. B. (2009) *J. Biol. Chem.* **284**, 32147-32157

82. Griep, M. A., and McHenry, C. S. (1988) *Biochemistry* **27**, 5210-5215

83. Ayyagari, R., Impellizzeri, K. J., Yoder, B. L., Gary, S. L., and Burgers, P. M. (1995) *Mol. Cell Biol.* **15**, 4420-4429

84. Williams, C. R., Snyder, A. K., Kuzmic, P., O'Donnell, M., and Bloom, L. B. (2004) *J. Biol. Chem.* **279**, 4376-4385

85. Bertram, J. G., Bloom, L. B., Turner, J., O'Donnell, M., Beechem, J. M., and Goodman, M. F. (1998) *J. Biol. Chem.* **273**, 24564-24574

86. Hingorani, M. M., Bloom, L. B., Goodman, M. F., and O'Donnell, M. (1999) *EMBO J.* **18**, 5131-5144

87. Johnson, K. A. (1992) Transient-state kinetic analysis of enzyme reaction pathways. in *The Enzymes* (Sigman, D. S. ed.), 3rd Ed., Academic Press, San Diego. pp 1-61

88. Bertram, J. G., Bloom, L. B., Hingorani, M. M., Beechem, J. M., O'Donnell, M., and Goodman, M. F. (2000) *J. Biol. Chem.* **275**, 28413-28420

89. Kuzmic, P. (1996) *Anal. Biochem.* **237**, 260-273

90. Gomes, X. V., Schmidt, S. L., and Burgers, P. M. (2001) *J. Biol. Chem.* **276**, 34776-34783

91. Sexton, D. J., Kaboord, B. F., Berdis, A. J., Carver, T. E., and Benkovic, S. J. (1998) *Biochemistry* **37**, 7749-7756

92. Zhuang, Z., Berdis, A. J., and Benkovic, S. J. (2006) *Biochemistry* **45**, 7976-7989

93. Alley, S. C., Shier, V. K., Abel-Santos, E., Sexton, D. J., Soumillion, P., and Benkovic, S. J. (1999) *Biochemistry* **38**, 7696-7709

94. Millar, D., Trakselis, M. A., and Benkovic, S. J. (2004) *Biochemistry* **43**, 12723-12727

95. Stukenberg, P. T., Studwell-Vaughan, P. S., and O'Donnell, M. (1991) *J. Biol. Chem.* **266**, 11328-11334

96. Zhuang, Z., Yoder, B. L., Burgers, P. M., and Benkovic, S. J. (2006) *Proc. Natl. Acad. Sci. (USA)* **103**, 2546-2551

97. Gomes, X. V., and Burgers, P. M. (2001) *J. Biol. Chem.* **276**, 34768-34775

98. Burgers, P. M., Kornberg, A., and Sakakibara, Y. (1981) *Proc. Natl. Acad. Sci. (USA)* **78**, 5391-5395

99. Johnson, A., Yao, N. Y., Bowman, G. D., Kuriyan, J., and O'Donnell, M. (2006) *J. Biol. Chem.* **281**, 35531-35543

100. Schmidt, S. L., Gomes, X. V., and Burgers, P. M. (2001) *J. Biol. Chem.* **276**, 34784-34791

101. Georgescu, R. E., Kim, S. S., Yurieva, O., Kuriyan, J., Kong, X. P., and O'Donnell, M. (2008) *Cell* **132**, 43-54

102. O'Donnell, M., and Kuriyan, J. (2006) *Curr. Opin. Struct. Biol.* **16**, 35-41

103. Green, C. M., Erdjument-Bromage, H., Tempst, P., and Lowndes, N. F. (2000) *Curr Biol* **10**, 39-42

104. Lindsey-Boltz, L. A., Bermudez, V. P., Hurwitz, J., and Sancar, A. (2001) *Proc. Natl. Acad. Sci. (USA)* **98**, 11236-11241

105. Mayer, M. L., Gygi, S. P., Aebersold, R., and Hieter, P. (2001) *Mol. Cell* **7**, 959-970

106. Majka, J., and Burgers, P. M. (2004) *Prog Nucleic Acid Res Mol Biol* **78**, 227-260

107. Hanna, J. S., Kroll, E. S., Lundblad, V., and Spencer, F. A. (2001) *Mol. Cell Biol.* **21**, 3144-3158

108. Naiki, T., Kondo, T., Nakada, D., Matsumoto, K., and Sugimoto, K. (2001) *Mol. Cell Biol.* **21**, 5838-5845

109. Bermudez, V. P., Maniwa, Y., Tappin, I., Ozato, K., Yokomori, K., and Hurwitz, J. (2003) *Proc. Natl. Acad. Sci. (USA)* **100**, 10237-10242

110. Bylund, G. O., and Burgers, P. M. (2005) *Mol. Cell Biol.* **25**, 5445-5455

111. Shiomi, Y., Shinozaki, A., Sugimoto, K., Usukura, J., Obuse, C., and Tsurimoto, T. (2004) *Genes Cells* **9**, 279-290

112. Kanellis, P., Agyei, R., and Durocher, D. (2003) *Curr Biol* **13**, 1583-1595

113. Bellaoui, M., Chang, M., Ou, J., Xu, H., Boone, C., and Brown, G. W. (2003) *EMBO J.* **22**, 4304-4313

114. Ben-Aroya, S., Koren, A., Liefshitz, B., Steinlauf, R., and Kupiec, M. (2003) *Proc. Natl. Acad. Sci. (USA)* **100**, 9906-9911

115. Bermudez, V. P., Lindsey-Boltz, L. A., Cesare, A. J., Maniwa, Y., Griffith, J. D., Hurwitz, J., and Sancar, A. (2003) *Proc. Natl. Acad. Sci. (USA)* **100**, 1633-1638

116. Parker, A. E., Van de Weyer, I., Laus, M. C., Verhasselt, P., and Luyten, W. H. (1998) *J. Biol. Chem.* **273**, 18340-18346

117. Majka, J., and Burgers, P. M. (2003) *Proc. Natl. Acad. Sci. (USA)* **100**, 2249-2254

118. Majka, J., and Burgers, P. M. (2007) *Cell cycle (Georgetown, Tex* **6**, 1157-1160

119. Yao, N. Y., Johnson, A., Bowman, G. D., Kuriyan, J., and O'Donnell, M. (2006) *J. Biol. Chem.* **281**, 17528-17539

BIOGRAPHICAL SKETCH

Jennifer Thompson was born in 1985 in Long Island, New York. The middle child of three children, she has an older brother and a younger sister. For the first 12 years of her childhood, she lived in the Poconos in Pennsylvania. In 1998, her family moved to Bradenton, Florida where she graduated from Lakewood Ranch High School in 2003. She earned her B.S. in microbiology and cell science from the University of Florida in 2007. In her last semester of her undergraduate career, Jennifer began research in Dr. Linda Bloom's biochemistry laboratory. She continued working in the lab as a technician until she started the master's program in the Biochemistry and Molecular Biology Department at U.F. in the fall of 2008. After completing the master's program, Jennifer will continue working on her research in Dr. Bloom's lab.